Energy band offsets of dielectrics on $InGaZnO_4$

David C. Hays, B. P. Gila, S. J. Pearton, and F. Ren

Citation: Applied Physics Reviews **4**, 021301 (2017); doi: 10.1063/1.4980153
View online: http://dx.doi.org/10.1063/1.4980153
View Table of Contents: http://aip.scitation.org/toc/are/4/2
Published by the American Institute of Physics

Articles you may be interested in

Bright narrowband biphoton generation from a hot rubidium atomic vapor cell
Applied Physics Reviews **110**, 161101161101 (2017); 10.1063/1.4980073

Perspective: Dissipative particle dynamics
Applied Physics Reviews **146**, 150901150901 (2017); 10.1063/1.4979514

A simulation study on the phase behavior of hard rhombic platelets
Applied Physics Reviews **146**, 144901144901 (2017); 10.1063/1.4979517

A microscopic mechanism of dielectric breakdown in SiO2 films: An insight from multi-scale modeling
Applied Physics Reviews **121**, 155101155101 (2017); 10.1063/1.4979915

APPLIED PHYSICS REVIEWS

Energy band offsets of dielectrics on $InGaZnO_4$

David C. Hays, B. P. Gila, S. J. Pearton, and F. Ren
Department of Materials Science and Engineering, University of Florida, Gainesville, Florida 32611, USA

(Received 2 March 2017; accepted 24 March 2017; published online 18 April 2017)

Thin-film transistors (TFTs) with channels made of hydrogenated amorphous silicon (a-Si:H) and polycrystalline silicon (poly-Si) are used extensively in the display industry. Amorphous silicon continues to dominate large-format display technology, but a-Si:H has a low electron mobility, $\mu \sim 1\,cm^2/V\,s$. Transparent, conducting metal-oxide materials such as Indium-Gallium-Zinc Oxide (IGZO) have demonstrated electron mobilities of 10–50 $cm^2/V\,s$ and are candidates to replace a-Si:H for TFT backplane technologies. The device performance depends strongly on the type of band alignment of the gate dielectric with the semiconductor channel material and on the band offsets. The factors that determine the conduction and valence band offsets for a given material system are not well understood. Predictions based on various models have historically been unreliable and band offset values must be determined experimentally. This paper provides experimental band offset values for a number of gate dielectrics on IGZO for next generation TFTs. The relationship between band offset and interface quality, as demonstrated experimentally and by previously reported results, is also explained. The literature shows significant variations in reported band offsets and the reasons for these differences are evaluated. The biggest contributor to conduction band offsets is the variation in the bandgap of the dielectrics due to differences in measurement protocols and stoichiometry resulting from different deposition methods, chemistry, and contamination. We have investigated the influence of valence band offset values of strain, defects/vacancies, stoichiometry, chemical bonding, and contamination on IGZO/dielectric heterojunctions. These measurements provide data needed to further develop a predictive theory of band offsets. *Published by AIP Publishing.*
[http://dx.doi.org/10.1063/1.4980153]

TABLE OF CONTENTS

I. INTRODUCTION

a-Si thin film transistors (TFTs) have become the staple of the flat panel industry.[1–3] There is great demand for ever-higher resolution, larger screen size, and lower power. However, delivering high-resolution, low-power displays with bright, true colors is challenging and has pushed traditional a-Si technology to its limits.[11–19] To continue the pace of display development, there is strong interest in new materials.[4–10,20–27] In recent years, amorphous oxide semiconductors (AOSs) have attracted much attention for use in flat panel displays and flexible TFTs due to their improved electrical and optical performance as compared to amorphous Si, which is still the dominant technology used in TFTs today.[1–6] Several AOS materials have been studied including In-Zn-O,[7–10,20–24] In-Sn-O,[23,25] Zn-Sn-O,[23,25] Zn-In-Sn-O,[17,23–25] and In-Ga-Zn-O (a-IGZO).[7–10,23–41] Among all AOS materials, a-IGZO has been the most widely investigated due to maintaining a very high electron mobility in the amorphous state (10–50 $cm^2\,V^{-1}\,s^{-1}$), and the wide controllability of carrier concentration through oxygen partial pressure during deposition.[8–10,22–26] Moreover, its ability to be deposited at room temperature allows for use of novel flexible substrates such as plastic or even paper, which raises the possibility of making low-cost electronics on a very wide range of arbitrary surfaces including plastic and

paper.[22–26,42–47] Amorphous IGZO TFTs are highly transparent and can be deposited uniformly over large areas, opening up potential applications as switches in the active-matrix and driver-integrated circuits of low cost flexible displays.[9,23–27] However, a major remaining issue with IGZO is a better understanding of the appropriate choice of compatible gate dielectrics for devices fabricated using IGZO channels.[9,23–27]

II. BACKGROUND

A. IGZO properties

There is great interest in using amorphous oxide semiconductors (AOSs) as the active layer of transparent TFTs.[23–27,42] Specifically, the ternary oxide system InGaZnO is one of the most promising candidates.[43–81] IGZO is a wide bandgap (~3.5 eV), n-type semiconductor and, as shown in Table I, it is the only material to combine high optical transparency and high carrier mobility with high yield and low cost.[1,5,8,23–27] Table I compares the properties of oxide semiconductors, amorphous Si, polycrystalline Si, and typical organic semiconductors.[1,10–19] Generally, covalently bonded semiconductors (e.g., Si) conduct through highly directional sp3 hybrid bonding.[11–19] Therefore, in the amorphous state, the electron path is distorted and results in decreased mobility.[11–19] However, in a-IGZO, conduction is through a metal ion's highly symmetrical s orbitals.[42,82] The high degree of symmetry allows the conducting path and carrier mobility to still be maintained even in the amorphous phase.[43–55,82]

Single-crystalline IGZO (sc-IGZO) has a complex, layered structure with alternating stacks of InO_2 and $GaO(ZnO)$[2,7,10,27,28] as shown in Figure 1.[76] Unlike binary ZnO, a-IGZO can have a uniform amorphous phase because In_2O_3 and Ga_2O_3 promote glass phase formation,[29,43–55,83] and the amorphous phase has been shown to be stable up to ~500 °C.[23] Many methods have been reported for a-IGZO deposition, including pulsed laser deposition (PLD),[23–31] but generally RF[20,25] or DC[37–39,84,93] sputtering are used due to their high deposition rate and excellent uniformity.

As illustrated in Figure 2,[24,50] in conventional, covalently bonded semiconductors, electrons conduct through highly directional *sp3* hybrid bonding,[43–55] as discussed above. When these semiconductors are in the amorphous state, the electron path is distorted by the resulting disorder and form deep localized states.[1,5,6,23,25,43–55] This results in the electrons or holes travelling by hopping, which significantly reduces carrier mobility and results in the low values shown in Table I.[23,25,43–55] These values contrast to single crystal Si, where the electron mobility is ~1450 $cm^2/V\,s$ in the intrinsic material at room temperature.[15] On the other hand, in a-IGZO, the electrons conduct through a metal ion's *s* orbital, which is highly symmetrical.[50] The high degree of symmetry allows the conducting path and carrier mobility to still be maintained even in the amorphous phase[50] (Figure 2 (Refs. 24 and 50)) To ensure a high mobility in the amorphous phase, a sufficient *s* orbital overlap between metal ions is necessary. To satisfy this requirement, Hosono *et al.*[50,52,82–84] proposed a model which predicts that the metal ions should be heavy, post transition metal cations with a large principal quantum number ($n \geqq 5$).[20,25] For example, the Hall mobility of the In-Ga-Zn-O system is primarily determined by the fraction of the In_2O_3 content[23] in agreement with the Hosono theory[20,25] since In^{3+} has the largest ionic radius ($n = 5$) among the metal cations.[43,49,50]

For a TFT to have a low off-state drain current and high on-to-off ratio, it is important to control the semiconductor channel carrier concentration to a low level.[4,5] In AOS films, carrier generation can occur via oxygen vacancy formation.[5,23] The incorporation of Ga^{3+} helps in suppressing oxygen vacancies in a-IGZO thin-films since it has a stronger bond to oxygen than Zn or In ions.[23,50] A comparative study between a-IZO and a-IGZO has also shown that a-IGZO has a five orders of magnitude larger reduction in carrier concentration than a-IZO when these materials are deposited under the same condition, as shown in Figure 3.[80]

Finally, though a-Si:H is widely used in TFT backplanes today, it is highly absorbing in the visible spectrum, with transmittance less than 30%.[11,14,17] This has been a major drawback for utilizing such material in optoelectronics and a-Si:H suffers from light-induced instabilities.[84–86] a-IGZO has a wide bandgap (~3.5 eV) and is highly transparent in the visible spectrum with transmittance over 90%.[7,9,10,23] The large difference between a-Si and a-IGZO allows for higher resolution, transparent displays at an equivalent transmittance.[23–27] The progress on improving the control of instabilities during biased operation of IZGO has also been impressive.[86–94]

B. Band offset importance

There are three main criteria that a gate dielectric must possess to be considered acceptable.[94–97] First, it must be thermodynamically stable with the semiconductor and not react

TABLE I. Comparison of TFT materials (data taken from Refs. 7 and 23–27 for IGZO, Refs. 11, 14, 17, 18, and 22 for amorphous and poly-Si, and Refs. 26 and 27 for organic TFTs).

TFT Properties	α-IGZO	α-Si	Poly-Si	Organics
Field effect mobility ($cm^2/V\,s$)	3–35 (Refs. 7, 23, 24)	0.5–1 (Refs. 11 and 14)	30–300 (Refs. 17 and 18)	~0.1 (Ref. 26)
Process temperature (°C)	RT (Ref. 24)	~350 (Ref. 17)	450 (Ref. 18)	<150 (Ref. 27)
Transparency (%)	>80 (Ref. 25)	<20 (Ref. 18)	<20 (Ref. 22)	>80 (Ref. 26)
Yield	High (Ref. 26)	High (Ref. 18)	Medium (Ref. 18)	Low (Ref. 26)
Manufacturing cost	Low (Ref. 26)	Low (Ref. 11)	High (Ref. 18)	Low (Ref. 26)
Long term TFT reliability	High (Ref. 27)	Low (Ref. 17)	High (Ref. 18)	Low in air (Ref. 27)
Substrate	Glass plastics paper (Ref. 27)	Glass (Ref. 22)	Quartz (Ref. 22)	Glass Plastics (Refs. 26 and 27)

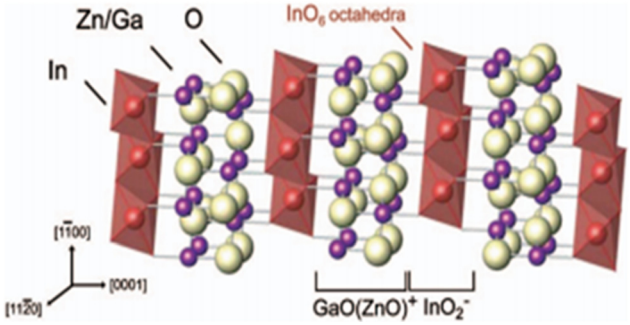

FIG. 1. Structure of single crystal $InGaZnO_4$ (reproduced from M. Orita *et al.*, Phys. Rev. B **61**, 1811 (2000). Copyright 2000 American Physical Society.

during processing. Second, it must provide a high quality interface with low defect and trap density to ensure high carrier mobility. Finally, it must act as a barrier to both electrons and holes which is among the most important physical parameters for a given heterojunction system.[94,98–103] Because these discontinuities can form a barrier for carrier transport across the interface, the knowledge of these quantities is essential for calculating the transport properties of the interface or the electrostatic potential in a heterojunction device. There are three types of band alignments: type I, type II staggered, and type III broken gap.[95,96]

The device concepts that can be implemented in a given heterojunction system will depend strongly on the type of band alignment and device performance dependent on the exact values of the band offsets.[23–27,98–110] Most Local Density Approximation/Density Functional Theory (LDA/DFT) approaches typically underestimate the bandgap, and hence, the conduction band offset (CBO) may be under/overestimated, but generally these theories perform well with the valence band offset (VBO) calculations.[94–96]

The energy band diagram of an oxide-semiconductor heterostructure represents a summary of the electronic structure of each material in the stack, and how they align with one another. The valence band is the highest occupied, allowed state and usually referred to as the valence band maximum (VBM). In a band diagram it is, typically,

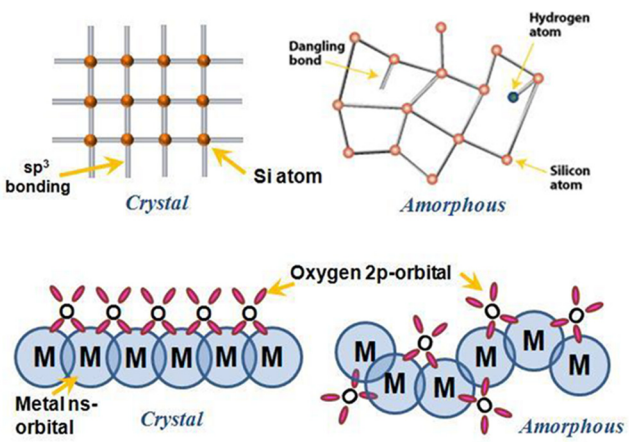

FIG. 2. Schematic orbital drawing of electron conducting pathway (conduction band bottom) in (a) conventional covalent bond semiconductors (e.g., Si) and (b) ionic oxide semiconductors (after Refs. 24 and 50).

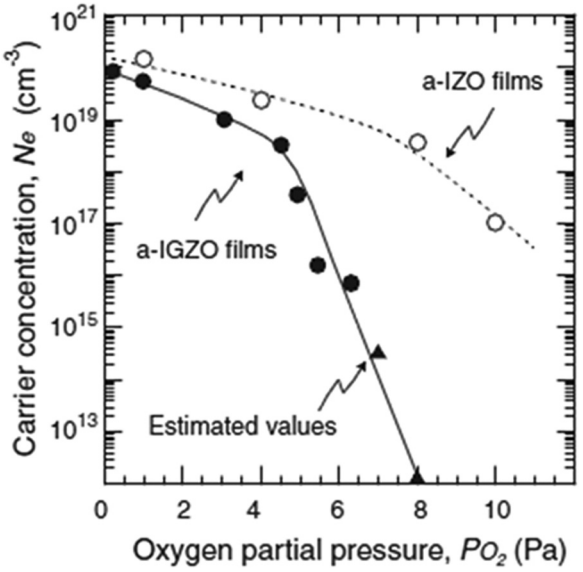

FIG. 3. Dependence of carrier concentration on oxygen partial pressure for a-IGZO and a-IZO films (reproduced from H. Hosono, J. Non-Cryst. Solids **352**, 851 (2006). Copyright 2006 Elsevier Publishing.

depicted by a line labeled by E_V. Likewise, the conduction band is the beginning of the upper band of allowed states. In a band diagram, it is represented by a line labeled by E_C, which represents the lowest possible energy state in the conduction band or the conduction band minimum (CBM). Figure 4 shows the band diagram for a Type I (straddled) band alignment. In this band diagram, the VBM and CBM of the oxide ($E_{V,OX}$ and $E_{C,OX}$) and those of the semiconductor ($E_{V,S}$ and $E_{C,S}$) are labeled.

If an electron occupying the bottom of the conduction band of the semiconductor were to move toward the oxide, the probability that it will be reflected increases as the barrier height increases. For sufficiently thin oxides, the probability will be 1 minus the tunneling probability. This is because

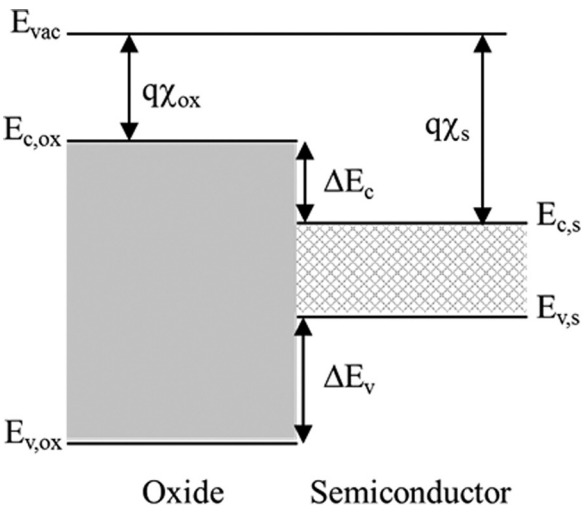

FIG. 4. Band diagram of a Metal-Oxide-Semiconductor (MOS) stack. E_{vac} is the vacuum level and E_C and E_V are the conduction and valence band energies, ΔE_C refers to the conduction band offset with the metal/oxide or semiconductor/metal with appropriate subscripts, ΔE_V refers to the valence band offsets in a similar fashion, q is the electronic charge, Φ refers to the respective work functions, and χ is the electron affinity of the respective layers.

there are no electronic states in the oxide at this energy for it to occupy. The difference between the oxide and the semiconductor conduction band maxima is the energy barrier to electrons in the semiconductor. This difference is called the oxide-semiconductor conduction band offset (CBO) and is labeled $\Delta E_{C,OS}$ in Figure 4. Similarly, the difference between the oxide and semiconductor valence band maxima is the valence band offset (VBO), which is labeled $\Delta E_{V,OS}$. This is the energy barrier that blocks the flow of holes from the semiconductor to the oxide. Thus, when attempting to reduce the gate leakage current there are two main factors that must be considered. The first is the physical thickness of the dielectric to reduce tunneling and the second is sufficiently large conduction and valence band offsets.

It is essential to understand the energy band structure at heterojunction interfaces. While there has been much work to date on IGZO devices with various gate dielectrics, there has been very little systematic work on determining the band offsets on such devices.[40,45,111–122] Generally, a new dielectric is employed without an actual knowledge of the relative condition and valence band offsets.[114–122] Two recent reviews of advances in AOS TFTs suggested that more work was needed on gate dielectrics development for next generation TFT devices.[23,24] Materials with a high dielectric constant (high-K) are desirable in IGZO TFTs, since the higher capacitance can reduce the effect of interface traps, and therefore reduce the device operating voltage.[23–27] However, many of the high-K dielectric choices available are often synthesized in polycrystalline form, which is undesirable due to impurity diffusion through grain boundaries and there are few choices with sufficiently high bandgap to get the desired >1 eV conduction and valence band offsets.[94,95]

C. X-ray photoelectron spectroscopy (XPS)

Obviously, the bandgap of the IGZO and the dielectric on top of it must be measured separately on thick samples of both materials. This is done usually for IGZO using either UV/Vis or reflection electron energy loss spectroscopy (EELS).[23–27] The valence band offset between the dielectric and IGZO is directly measured and the conduction band offset is derived from this and the differences in bandgaps.[124,125] One of the key methods for determining valence band offsets is XPS in conjunction with techniques for obtaining bandgaps, like absorption or various types of electron energy loss spectroscopies,[126–138] so it is worth briefly reviewing the need for accounting for sample charging in dielectrics and curve fitting of the data. Nichols *et al.*[134] provide a discussion of the precision of the XPS approach in determining core levels. This depends on a number of factors, including the linewidth of the x-ray source employed, charging effects, and the resolution of the electron analyzer, which includes the geometry and so-called pass energy of this analyzer.[135,136]

XPS measures the binding energies of the atomic core-level electrons of materials and the output is so-called core-level spectra which are due to the specific chemical composition in the near-surface region. The depth over which these spectra are acquired is determined by the escape depth of the excited electrons and is typically of order a hundred angstroms. Beyond the chemical composition of the surface region, XPS can also be used to determine the bandgap energy near the surface of the sample.[131–134] Charge compensation in most XPS experiments is performed using an electron flood gun since the dielectrics are insulating. A charge compensation flood gun is often not sufficient at eliminating all surface charge, and additional corrections must be performed. Using the known position of the adventitious carbon (C-C) line in the C 1s spectra at 284.8 eV, charge correction was performed. An optimized peak fit to the carbon 1s spectrum on IGZO is shown in Figure 5. Using a simple peak model involving a single C-C peak at 284.8 can lead to errors of 0.5 eV or more. Therefore, additional peaks are generally added. In our work, we add one peak constrained to be 1.5 eV above the main peak and of equal full width at half maximum (FWHM). This higher binding energy peak is ascribed to alcohol (C-OH) and/or ester (C-O-C) functionality. A further high binding energy peak, attributed to O-C=O, is added with a position constraint of 3.7 eV above the main peak. All peaks are constrained to a peak area ratio of 2:1:1.

The basic experimental approach when measuring XPS spectra and checking for the presence of charging effects is to look at the deltas between peaks (not individual peaks) with the flood gun on and off. If the deltas diverge from accepted values, then the analyst uses the flood gun to get them to the accepted (non-charging) values. In general, XPS analyses for IGZO/dielectrics that have been published in the literature have not used a specific procedure to handle differential charging, where there is a difference in the amount of charging between the dielectric and the underlying semiconductor, other than using the flood gun to compensate the deltas from one of the layers. In all of our work to date, we have found that charging and differential charging are not significant problems with the configuration and samples used. For charging, for example, we have noted that in our data sets, if we removed the C1s corrections, it only changed the offsets in the hundredths of eV range. This is a very small correction compared to the offsets themselves. Similarly, differential charging due to the different conductivities of the dielectric and the substrate, which is often a significant issue with

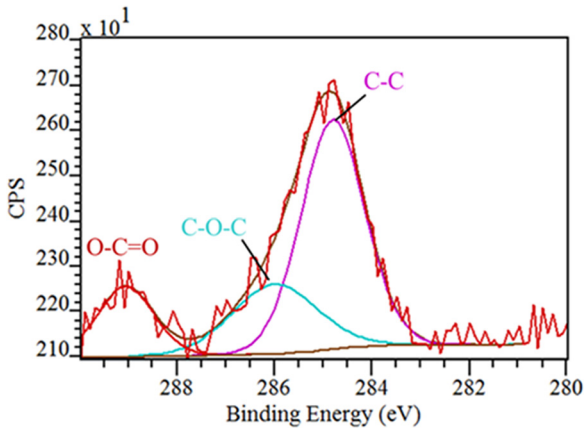

FIG. 5. Optimized peak fit of carbon 1s spectra.

dielectrics on conducting substrates with relatively small bandgaps like Si,[139] has not been found to be a problem with measurements on IGZO to date with the relatively small number of dielectrics, thicknesses, and conductivity levels in the IGZO that have been examined. This may be a result of the relatively large gap of IGZO (~3.5 eV), leading to much smaller differences in conductivity relative to the case of Si and its dielectrics. In general, the procedure for handling dielectric materials is not to get a net zero charge but to wait for the peak positions to stabilize.

Bersch *et al.*[139] published a detailed study of the band offset of the $HfO_2/SiO_2/Si$ system using charge corrected XPS. This is a very technologically relevant system.[140] Their study found that after correction for charging, the valence band offsets in this system were smaller than the values for uncorrected XPS analysis and in fact were in strong agreement with the values measured by UV photoemission spectroscopy and internal photoemission.[139,141] They recorded their XPS spectra after at least 6 min of x-ray exposure to ensure charge saturation, which was sufficient to be beyond the initial period when the samples displayed charging and shifting of peaks to higher energies. This increase in binding energies can occur due to the charging created by holes created by the ejection of photoelectrons accumulating in the sample.[142] Bersch *et al.*[139] found that the charging-induced shift in the HfO_2 spectral features was always larger than for Si, which they interpreted as arising from differential charging between the components of the dielectric/Si stack.[139] They discussed methods for correcting for this differential charging by taking into account the depth-averaged energy shifts in the peaks of each component spectrum. The corrections in charging shifts in HfO_2 were significant (0.60–102 eV depending on the thickness), and in the SiO_2/Si system, the charging shift for Si was 0.20 eV and for SiO_2S was 0.47 ± 0.03 eV.[139] The net effect for the valence band offset of HfO_2/Si was of order 0.5 eV.[139]

The differential charging is clearly simple and material-dependent and might become more significant with higher resistivity dielectrics (i.e., larger gap) or stacked structures incorporating multiple dielectrics with differing gaps, or with dielectrics of greater thickness, which could be the case as one goes to higher-K materials. It is certainly an issue worth monitoring for as IGZO/dielectric technology matures. There are analytical methods for correction from the work by Bersch *et al.*[139] and physical methods to electrically isolate the entire sample, thereby eliminating the conductive film from gaining any lost electrons. The sample will float to some potential but there is no shift in the delta core levels.

1. Background and peak/curve fitting

Photoemission spectra contain a background formed principally by inelastic scattering of photoelectrons.[135–138,143–152] This effect is typically observed as a step-like increase in the baseline after passing through a core level peak. In order to perform a qualitative elemental analysis, peak shape analysis, or a comparison to a theoretical DOS, background subtraction must be performed. The most commonly applied backgrounds are linear, Shirley[124] or Tougaard.[126,127] The Shirley background is calculated iteratively depending on the integral of the spectrum at lower binding energy, and a constant parameter is then adjusted to align the ends of the background with the data at points chosen to enclose the feature of interest. This results in a step-like background.

In our case, we typically use low-resolution survey scans (to examine the surfaces of the films and to determine elemental composition) and then perform very high resolution spectra (multiplex, to determine the binding energy of specific elements). The low resolution survey scans are performed to identify peaks for high resolution analysis (core analysis peaks and contamination). A typical electron pass energy at 187.5 eV is used in our experiments. Charge correction is performed using the known position of the C-(C,H) line in the C 1s spectra at 284.5 eV. The valence band maximum (VBM) is determined by using a linear extrapolation method, i.e., it is determined by linear fitting the leading edge of the valence band and linearly fitting the flat energy distribution and finding the intersection of these two lines. The core-level peaks were referenced to the top of valence band for the thick IGZO and the thick film of dielectrics. To determine the valence band offset, the binding energy differences between the valence band and the selected core peaks for the single thick layers were combined with the core-level binding energy differences for the heterojunction sample. Spectra from insulating samples can be charge corrected by shifting all peaks to the adventitious C 1s spectral component (C-C, C-H) binding energy set to 284.8 eV. The C1s spectrum typically has C-C, C-O-C, and O-C=O components and optimization involves constraining these additional peaks. This charge correction is used for chemical analysis, but not band offset measurements.

Peak widths are determined by the core-hole lifetime, the linewidth of the radiation source, and the instrumental resolution of the analyzer. The Heisenberg uncertainty relationship allows us to determine the peak width due to core-hole lifetime as[132–135]

$$\Gamma = \frac{\tau}{h}, \tag{1}$$

where Γ is the peak width, h is Planck's constant, and τ is the core-hole lifetime in seconds. Γ is generally larger for inner shell orbitals as an inner shell core hole may be filled by any of the outer shell electrons, so the core-hole lifetime is shorter.[136] Also Γ increases with the atomic number as the valence electron density increases, so there are more electrons to fill the core holes. The contribution due to core-hole lifetime produces a Lorentzian line shape.[126–130,133,134]

In addition, the instrument resolution also plays a part, and this contributes a Gaussian broadening to the experimental peaks.[132] For XPS spectra in a narrow energy range (<20 eV), the instrumental resolution and thus the Gaussian peak width are assumed to be constant. The instrument is expected to have very similar resolution over such a small energy range. Spectral deconvolution is achieved using CASA XPS software with a curve-fitting process based on a constant Lorentzian (core-hole lifetime) broadened by a Gaussian (instrument resolution) with a ratio of 30:70. The

shapes of the peak (height, width, and Gaussian/Lorentzian function) are automatically varied until the best fit to the observed spectrum is achieved, as shown in Figure 6. Constraints (e.g., the shape and position of peak) can also be applied to peaks so that the results of the fitting process remain physically realistic. One note of caution is that we have seen that in some studies that the "true" adventitious carbon peak position is not the same on all materials although it is the most used correction for charging.

D. Electron energy loss spectroscopy (EELS)

Both REELS (reflection-EELS) and XPS EELS are commonly used to measure the bandgap of oxide dielectrics. Reflection electron energy loss spectroscopy (REELS) consists in bombarding the surface of a sample with a beam of monoenergetic electrons and detecting the energy distribution of the backscattered electrons.[143,145–148] When electrons enter a solid, they interact with the constituent atoms through Coulomb interaction. As a result, some electrons are scattered and the direction of their momentum is changed, and in some cases, they transfer energy to the sample.[146–149] A majority of incoming fast electrons will be elastically scattered from the atomic nuclei in the sample and deflected by a large angle.[143,144] In addition, some incoming fast electrons will be inelastically scattered from the atomic electrons. In such events, an incoming fast electron transfers a part, or all, of its energy to the atomic electron causing it to make a transition to a higher energy state. Low energy electron transitions in a solid, called the outer-shell transitions, are the ones studied in REELS.[143–147] Some outer-shell inelastic processes in REELS can be understood in terms of single electron excitations from the occupied states in the valence band to the unoccupied states of the conduction band.[141,143] This type of the transition requires energies on the order of 1 to 10 eV. As opposed to single electron excitations, the excitations of valence electrons can involve many electrons.[132] This collective effect is known as plasmon resonance and it is usually depicted as an electron density oscillating with respect to the stationary positive ion background in a solid.[143,144] For a majority of solids, plasmon excitation energies lie in the range between 5 and 30 eV.[132] Depending on the region of the sample where plasmons are excited, they are either called bulk or surface plasmons, where surface plasmons are restricted to a few surface layers of atoms. Since plasmons require electrons in the material to freely move, these types of outer-shell excitations will be important for the materials where electrons behave as free particles, like metals.[143,144] In materials in which electrons are localized, plasmon excitations are weak or nonexistent. In general, a REELS spectrum will consist of two main regions, as shown in Figure 7.[143,147] First, there is a primary or zero-loss peak that includes elastically or quasi-elastically scattered electrons. Second, there is the low energy loss region that includes the outer-shell excitations of valence electrons, i.e., single electron and/or plasmon excitations.[143,145]

In the case of metals, the most prominent features in the low energy loss region of the REELS spectrum will come from the surface and bulk plasmon excitations.[145] However, in the case of the metal oxides, the most prominent features are attributed to the excitations of electrons across the bandgap or the gap between the highest occupied molecular orbital (VBM) and the lowest unoccupied molecular orbital (CBM).[143] In the work on dielectrics of interest for IGZO, the focus is on electronic interactions, which can be performed with an experimental resolution of typically 0.5–1 eV estimated from the full width at half maximum (FWHM) of the elastic peak.

While the UV/Vis technique requires relatively thick films (>0.5 μm) to determine the bandgap, REELS has the advantage of only needing a thicker film than the sampling depth, so only a few nanometers are actually required. In addition, while our UV/Vis has a cutoff at ~6 eV, the REELS technique has no such upper limit which makes it ideally suited to study dielectric materials.

We have typically used the XPS-REELS variant. The measurement of the dielectric bandgap is done using the onset of electron energy loss spectra. The energy corresponding to the onset of inelastic losses is found by extrapolating the linear-fit line and calculating its intersection with the "zero" level. The bandgap is the difference between the centroid of elastic scattering and the calculated intersection. In our case, the samples were placed in the same XPS system and REELS spectra were obtained by using a 1 kV electron beam and the hemispherical electron analyzer. Following the

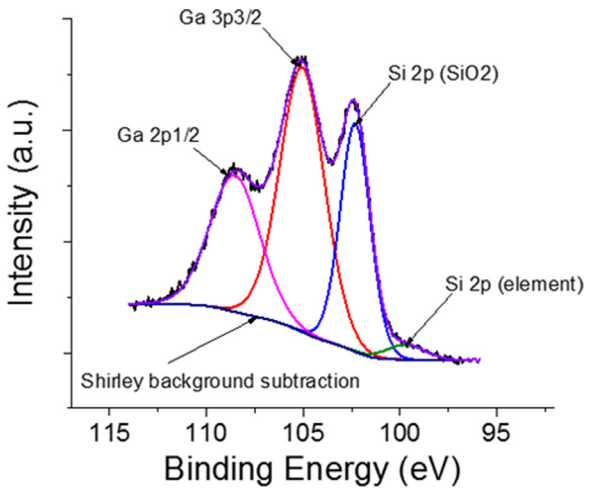

FIG. 6. XPS spectra showing peak fitting elements.

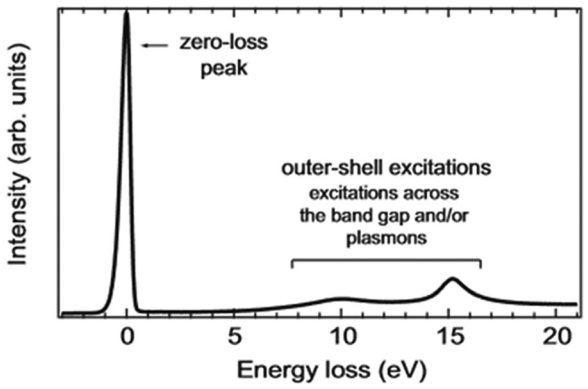

FIG. 7. Typical REELS spectrum.

photoelectric excitation of bound electrons, the outgoing electrons can suffer inelastic losses to collective oscillations and single particle excitations. The collective excitations, plasmons, show up as broad, smooth replicas of the photoelectron peaks shifted to lower kinetic energies. The onset of single particle excitations can also be observed in the form of a step at an energy equal to the bandgap Eg below the core level. Therefore, the band-gap can be found by drawing a linear fit line with the maximum negative slope from a point near the onset of the loss signal spectrum to the background level, as shown in Figure 8. The energy corresponding to the onset of inelastic losses is found by extrapolating the linear-fit line and calculating its intersection with the "zero" level. The bandgap is the difference between the centroid of elastic scattering and the calculated intersection. The precision of finding the bandgap is limited because the slope of the loss feature may not very different from that of the background of the XPS spectrum, making background subtraction difficult. One issue we have noticed in measuring bandgaps of dielectrics with REELS is the effect of contamination from carbon and water, as well as defects. These can lead to high backgrounds in the spectrum, creates a higher energy shoulder, or can "smear" the energy distribution. The onset of energy loss then becomes difficult to distinguish and a traditional fit to a horizontal line may give lower values, and fitting to a lower slope can give artificially higher values of the bandgap. An example is shown in Figure 9 for sputtered $HfSiO_4$, where the presence of disorder leads to ambiguity in obtaining the bandgap, whereas dielectrics deposited by Atomic Layer Deposition (ALD) is well defined, as shown at the bottom of Figure 9.

E. Bandgap determination

The UV/Vis absorption technique measures the percent of light transmitted (%T) through a sample as a function of wavelength. Thin films (>0.5 μm) were deposited on quartz substrates in order to maximize transmission. A reference sample of the same substrate was used to remove the losses contributed by the substrate. To extract the bandgap, the optical absorption coefficient (α) is calculated[154,155]

$$\alpha = -\frac{1}{d} ln(T), \tag{2}$$

where d is the thickness and T is the ratio of transmitted (I) to the reference intensity (I_o). The bandgap is related to the optical absorption coefficient in the following way:[156–158]

$$(\alpha hv)^2 = (hv - E_g), \tag{3}$$

where hv is the energy, α is the absorption coefficient, and E_g is the optical bandgap. Thus to extract the bandgap, one must plot $(\alpha hv)2$ on the y-axis and hv on the x-axis. The band-gap energy (E_g) of the thin film can be obtained by utilizing the Tauc method[154,155] and extrapolating the linear portion of the curves relating $(\alpha hv)^2$ and hv to $(\alpha hv)^2 = 0$, as shown in Figure 10. In principle, there should be no absorption below the band edge and it should steeply increase when the photon energy approaches to Eg. In practice, just below Eg, α starts increasing slowly with increasing photon energy. Any defect or disorder in the system gives rise to localized energy levels

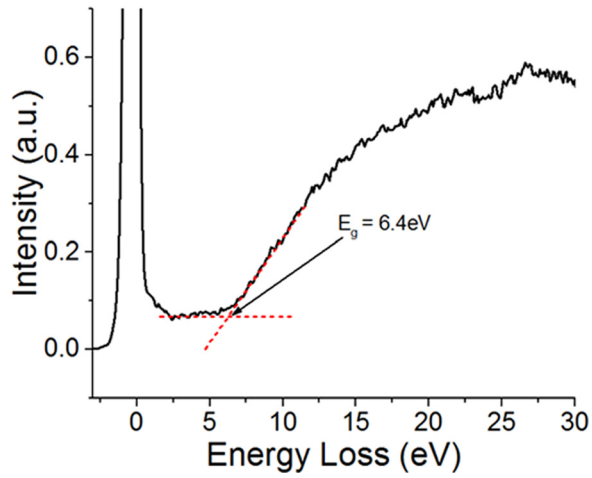

FIG. 8. Bandgap determination using linear fits to REELS spectrum.

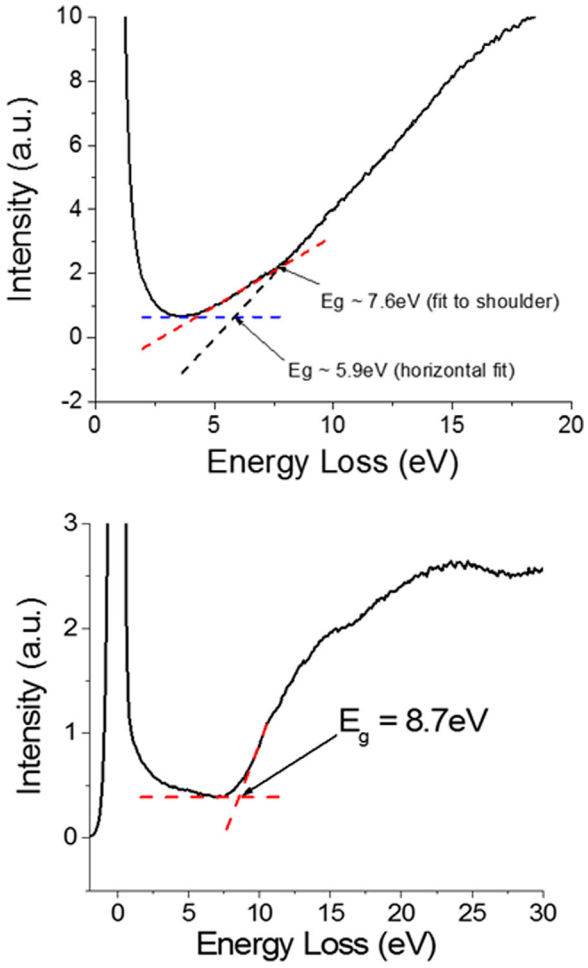

FIG. 9. Bandgap measurements of (top) sputtered $HfSiO_4$ with various fit methods of REELS spectra with indistinct onset energy loss that produces ambiguity in determining the bandgap by different extrapolation methods and (bottom) ALD SiO_2 showing the absence of shoulders due to contamination or defects.

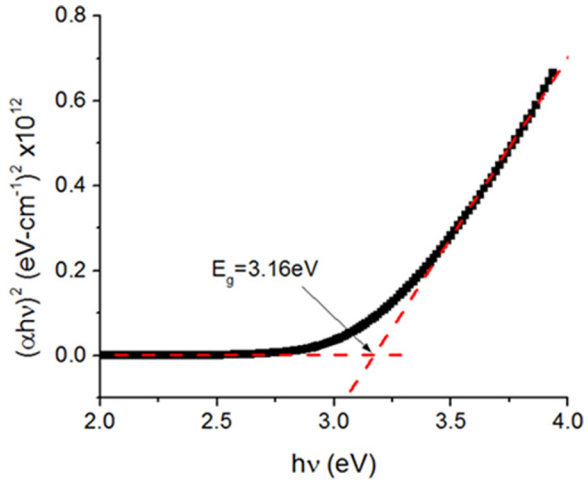

FIG. 10. Tauc plot of IGZO and linear fits to UV/Vis data to determine the bandgap.

within the bandgap or discrete states and this produces a band tailing effect.[136,146–150]

F. Determination of band offsets

Numerous experimental methods are used to determine the oxide/semiconductor band alignment. These include external photoemission spectroscopy,[133,149] internal photoemission spectroscopy,[150,151] and XPS core-level based method. The method of Kraut *et al.*[123,153] using x-ray photoemission spectroscopy has been established as a reliable way to determine band offsets at the hetero-junction interface. This method has also been successfully used to provide insights into interfacial properties between different materials.[153,159] It is based on using an appropriate shallow core-level position as a reference. Generally, this approach is based on the assumption that the energy difference between the core-level positions and valence-band maximum (VBM) is both fixed in the bulk.

The basic method, shown in Figure 11, is to first measure the energy difference between a core level and the VBM for both the single layer dielectric and semiconductor of interest.[54] One measures the reference core level binding energies in thick films of each material and then measures the binding energy difference between the two reference core levels in the heterojunction. The determination of ΔEv comes by combining those three quantities. Heterojunction samples, consisting of a thin (1–2 nm) layer of dielectric deposited on the semiconductor, are prepared in which the separation between reference core levels in each material is measured. The separation between the reference core levels can be translated directly into a value for the valence band offset (VBO) using the previously measured single layer sample core-level to VBM energies by the following relationship:

$$\Delta E_V = (E^1_{core} - E^1_{VBM})_{IGZO} - (E^2_{core} - E^2_{VBM})_{Dielectric} - (E^1_{core} - E^2_{core})_{Heterostructure}. \quad (4)$$

In a typical photoelectron spectrum, the onset of photoelectron intensity closest to the Fermi energy (E = 0)

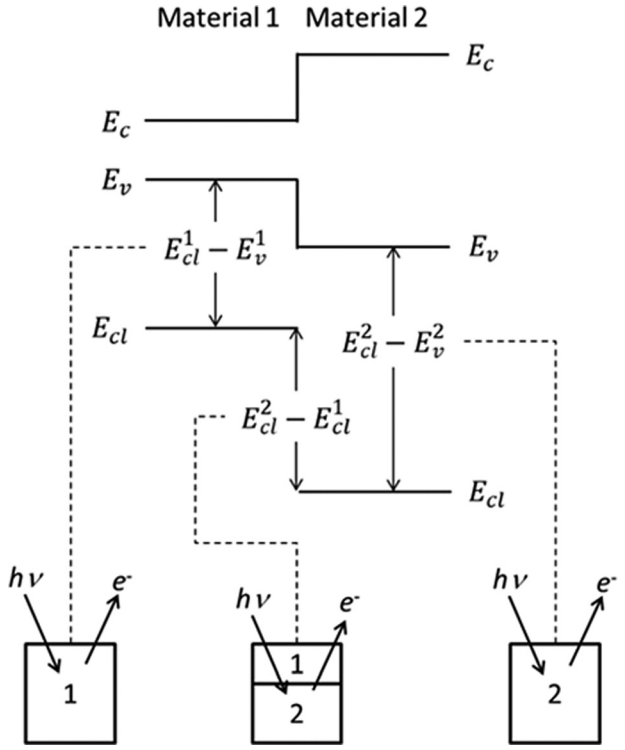

FIG. 11. A schematic energy band diagram illustrating the basic principle of XPS band offset measurements (for more details see Refs. 123 and 149).

generally corresponds to the photoemission of electrons from the VBM or the highest occupied state. To determine the VBM position, this rise in intensity is fit to a line and where that point intersects the baseline is reported as the VBM, as shown in Figure 12. We should also point out here that there are other methods beyond the linear extrapolation method for locating the VBM in XPS data such as fitting the spectra to a broadened density of states, as summarized in the study by Poveda and Glachant.[128] This compares the accuracy of different methods and concludes that the straight line method performs well as the more involved methods. It is interesting to note in that paper that, early on, the reported values of the band offset for the Si/GaAs

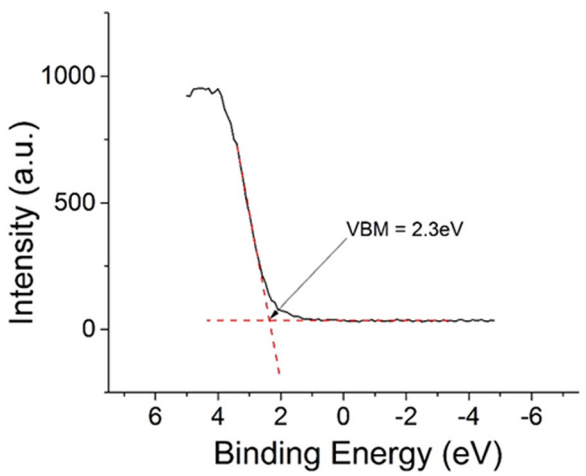

FIG. 12. Linear fit of the valence band edge of IGZO to determine the valence band maximum.

system measured by photoemission ranged from 0.05 to 0.70 eV.[128] The authors did a systematic study of potential sources of these variations, including changing the overlayer crystalline order, strain, and chemical reactivity.[128] They found the offset to be 0.23 ± 0.05 eV for both amorphous and crystalline overlayers, either strained or unstrained, with discontinuities up to 0.7 eV for room temperature growth.[128] These large discontinuities were found to be due to dangling bond states which altered the apparent valence band maximum energy. Their conclusion was that the discontinuity was more dependent on the interpretation of the data than on technological variations but that photoemission can yield accurate and single valued measurements of the valence band discontinuity.[128]

To determine the conduction band offset, it is necessary to measure the bandgap of each material. The samples are measured via UV/Vis or REELS, and the conduction band offset is calculated as follows:

$$\Delta E_C = E_g^{dielectric} - E_g^{IGZO} - \Delta E_V. \quad (5)$$

From these values, it is then possible to construct the flat band diagram and determine if this is a Type I, II, or III heterostructure.[160]

For the core level referencing approach of Kraut[123,153] used to determine the band alignment between IGZO and the various dielectrics, charge compensation is not relevant. The elegance of the Kraut method is that all the peak positions are relative. If the sample charges up by 10 eV, then that 10 eV offset will cancel out in every step of the Kraut measurement because each measurement consists of measuring the position of one core level relative to another. The two things that are most important in the Kraut method of determining band alignments are (1) linearity/calibration of the binding energy scale and (2) accounting for possible differential charging between the bottom and top films. Calibration of the binding energy scale is important because one is typically referencing the valence band maximum or a shallow core level to a deeper core level. If the 0–1000 eV binding energy scale is out of calibration by 1 eV, that error will propagate in the valence band offset measurement.

To summarize, charge compensation in XPS is needed for chemical analysis but not valence band offset measurements. Differential charging is an important consideration in photoemission based band offset measurements on the material that is insulating and the other has some conductivity, the need for charge compensation in XPS measurements of insulating dielectric samples. This is important if one is attempting to perform chemical analysis of a dielectric film based on XPS peak positions. Calibration of the binding energy scale is important because one is typically referencing the valence band maximum or a shallow core level to a deeper core level. If the 0–1000 eV binding energy scale is out of calibration by 1, i.e., that error will propagate in the valence band offset measurement.

G. Candidate materials as dielectrics for IGZO

High-k materials have been under investigation since the late 1990s in the silicon industry to identify those best suited to replace SiO_2 as the gate dielectric in MOSFETs.[94–96] As discussed previously, the primary criteria on which high-k materials are evaluated are dielectric constant, thermal and chemical stability in contact with the semiconductor, and the band offsets.[94–96] The dielectric constant should be high as possible to be useful for scaling of device sizes, but often a material with a high dielectric constant has a smaller bandgap and, consequently, smaller band offsets.[23–27] It is also necessary to have available deposition techniques that are compatible with standard TFT processing.[161–171] Figure 13 shows the bandgap versus dielectric constant of a number of high-k oxide candidate materials for IGZO.[96] The wider bandgap of IGZO limits the number of possible choices relative to materials such as Si with smaller bandgaps.

Band alignment at the oxide-semiconductor interface is important because the transport properties at the heterojunction interface are determined by the electronic band profiles at the interface.[172–177] The difference between the two valence band edges of the hetero-interface, valence band offset (VBO), serves as a barrier to prevent holes tunneling through the interface, while the difference between the two conduction band edges, conduction band offset (CBO), provides a barrier to minimize electron tunneling.[177,178] In order to effectively minimize carrier tunneling through the gate dielectric due to thermal fluctuations or quantum tunneling effect, Robertson suggested a rule-of-thumb that the VBO and CBO must be larger than 1.0 eV.[94–96]

Based on the specific requirements of IGZO, the high-k dielectrics with VBO or CBO with IGZO that will obviously be much smaller than 1 eV were not be considered for further investigation because of the large tunneling current.[179] Information on band offsets at the interfaces of high-k oxides and IGZO is still in its infancy. Since IGZO has a bandgap of ~3 eV, suitable gate dielectrics should have a bandgap of over 5 eV to meet the minimum requirement for a 1 eV band offset previously described. Based on this information, the best candidate dielectrics with bandgaps greater than 5 eV were investigated and these are listed in Table II.

III. IGZO BAND OFFSET LITERATURE REVIEW

While many IGZO TFT devices have been studied in recent years,[40–51,180–210] there has been less work done on

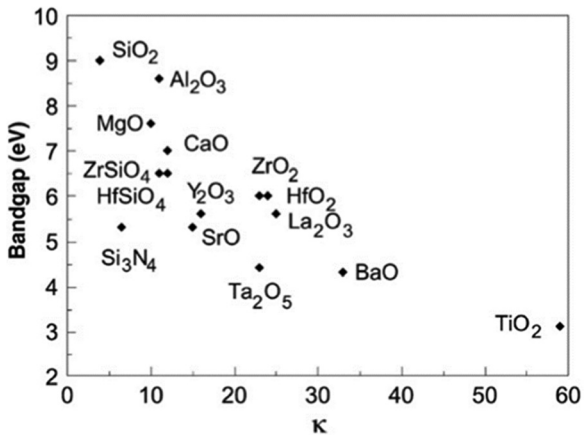

FIG. 13. Dielectric constant (κ) versus bandgap for oxides (after Refs. 94–96).

TABLE II. Properties of dielectric films that are candidates for gate materials on IGZO and whose band offsets are discussed in this work. Bandgaps and dielectric constants taken from Refs. 94–96.

Material	Bandgap (eV)	Dielectric constant
La_2O_3	5.5	21–30
HfO_2	5.7	15–26
$LaAlO_3$	5.9	24
Sc_2O_3	5.9	14
$HfSiO_4$	6.2	12
$ZrSiO_4$	6.7	11
SiO_2	8.9	4

determining the band offsets of these materials. The SiO_2/IGZO system first was studied by Douglas *et al.*[180] and was found to have strong carrier confinement due to the nested (Type 1) interface and large SiO_2 bandgap, as shown at the left of Figure 14. The PECVD SiO_2 film was deposited on Si and IGZO films at 300 °C and this produced a VBO of ~1.43 eV. In addition, Tahir *et al.*[181] performed a detailed study of the SiO_2/IGZO interface as a function of Ga content of the IGZO film. The IGZO bandgap increased with the Ga content, due to the higher bandgap of Ga_2O_3, which caused the VBO to be shifted down. In comparison, the ratio of 1:1:1 (In:Ga:Zn) is the same material deposited by Douglas[180] and can be directly compared as shown in Figure 14. It was not stated if this was a PECVD, thermal, or other type of oxide. It is interesting to note that the IGZO films were deposited on the SiO_2, which is the opposite to the work by Douglas.[180] There is close agreement in the data for bandgap values for both materials. However, there is a 0.5 eV difference in the reported VBO which points to the importance of processing methods on resulting offsets. Because IGZO was not subjected to high temperatures or high energy plasmas in the experiments where it was deposited on Si, there could be differences in the defect states which could cause shifts due to polarization at the interface. In addition, the VBM that Douglas reported was effectively annealed at 300 °C during the PECVD deposition.

The band offsets for Al_2O_3/IGZO have been studied by Cho *et al.*[182] and were determined to have a nested (Type 1) interface with offsets of 2.35 eV and 0.95 eV for the CBO and VBO, respectively, as shown in Figure 15. It was also noted that both the alumina film and IGZO were determined to be oxygen deficient which could have an impact on the band

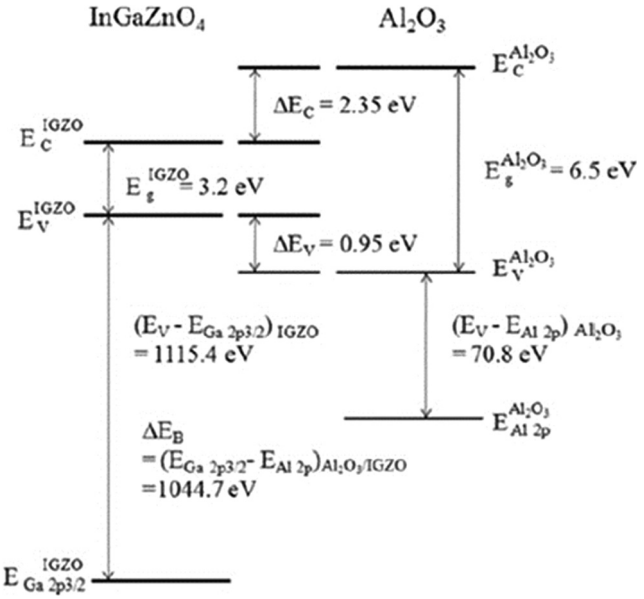

FIG. 15. Energy band diagram of a thin Al_2O_3/IGZO heterojunction interface (after Ref. 182).

offsets. The oxygen deficiency was determined by peak fitting the asymmetrical O1s spectra with two Gaussian-Lorentzian peaks and attributing one peak to the metal oxide and the other peak to the oxygen deficient material (vacancies). While there are most likely oxygen vacancies present in both the materials, the O1s spectra are not the proper peaks to investigate due to the always present carbonates. A more relevant method would be to investigate the Al 2p peak for asymmetry, which will indicate the presence of both Al-Al bonds and Al-O bonds. The high offsets result in excellent carrier confinement, even though it is smaller than that achieved with SiO_2.

The ZrO_2/IGZO heterojunction was found by Yao *et al.*[183] to have a nested interface but with no valence band offset as shown in Figure 16. With a CBO of 2.7 eV, the material would be an excellent barrier to electrons but no barrier to holes. A low valence band offset could affect the stability of a device during negative gate voltage.

A strong candidate material that has been well characterized and implemented in silicon IC manufacturing is HfO_2, due to its large dielectric constant and good thermal stability. This material was again studied by Cho *et al.*[108] and was found to have the CBO and VBO of 2.39 eV and 0.48 eV, respectively, as shown in Figure 17.

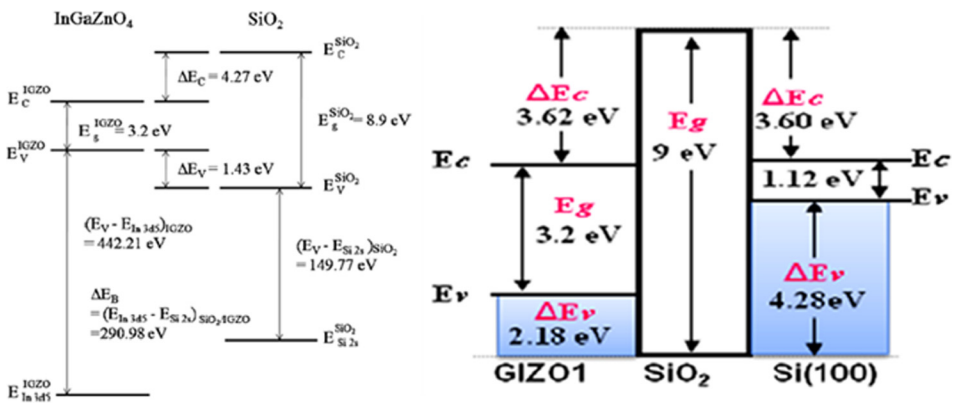

FIG. 14. Energy band diagram of a thin SiO_2/IGZO heterojunction interface (after Ref. 180).

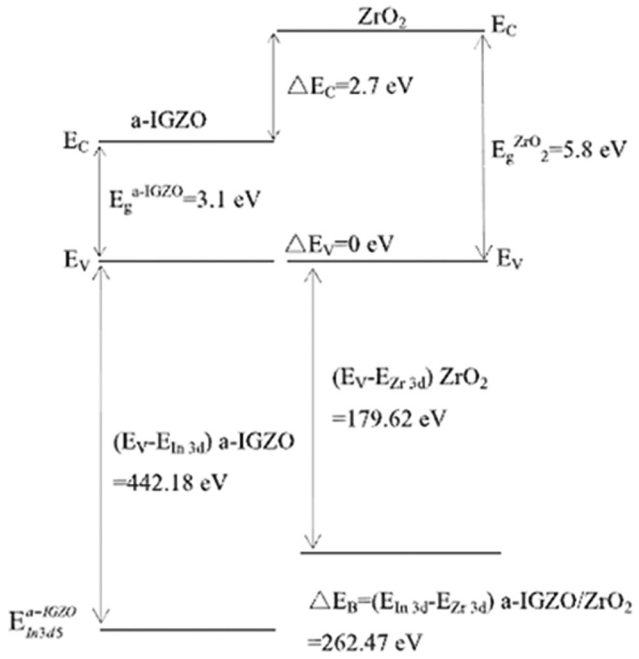

FIG. 16. Energy band diagram of a thin ZrO_2/IGZO heterojunction interface (after Ref. 200).

The Y_2O_3-stabilized ZrO_2 (YSZ)/IGZO interface was studied by Kim *et al.*[184] and was found to have a nearly perfectly symmetrical, nested band alignment. The lower bandgap of YSZ produced smaller offsets of 0.63 eV and 0.57 eV for the CBO and VBO, respectively. Despite the decreased band offsets, the symmetrical alignment allows for good carrier confinement at low voltage driving conditions.

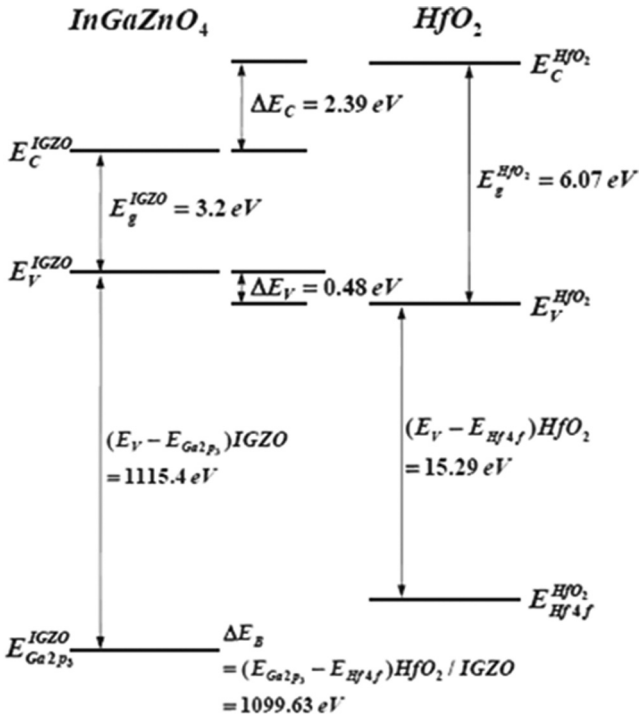

FIG. 17. Energy band diagram of a thin HfO_2/IGZO heterojunction interface (after Ref. 188).

A. New experimental determinations of band offsets

We deposited IGZO films by sputtering at room temperature on both Si and quartz by RF magnetron sputtering using a 3-in. diameter single target of $InGaZnO_4$. The RF power was 150 W, while the working pressure was constant at 5 mTorr in a pure Ar ambient. These films were then used as templates for deposition of different dielectrics by sputtering or ALD.

1. $HfSiO_4$

Hafnium silicate, $HfSiO_4$, is a high-k ($k \sim 15$–18) dielectric that is attractive for advanced metal-oxide semiconductor transistors because of its thermodynamic stability with silicon. The fact that it is well-characterized and deposition processes by a wide variety of methods are available makes it an attractive possibility for gates on IGZO TFTs. We found that the $HfSiO_4$/IGZO system has a staggered type-II alignment. This means that it will not be an appropriate choice as a gate dielectric on TFT structures but it may still be an effective surface passivation material on these devices. Figure 18 shows the band diagram of the $HfSiO_4$/IGZO heterostructure for samples kept in a vacuum during the entire deposition cycle. This system has a staggered, type II alignment, with a valence band offset of $-0.43\,\text{eV} \pm 0.04\,\text{eV}$ for samples in which all the layers were kept in a vacuum or -0.27 eV for samples exposed to atmosphere prior to the measurement. The respective conduction band offsets are then 3.07 eV for the vacuum samples and 3.01 eV for the vented samples.

The $HfSiO_4$/IGZO heterostructure is not a candidate as a gate for TFTs where we need positive offsets in both the valence and conduction bands but might still have application as a passivation layer on IGZO-based devices. The sample history in terms of exposure to atmosphere has a measurable effect on the resultant band offsets and issues

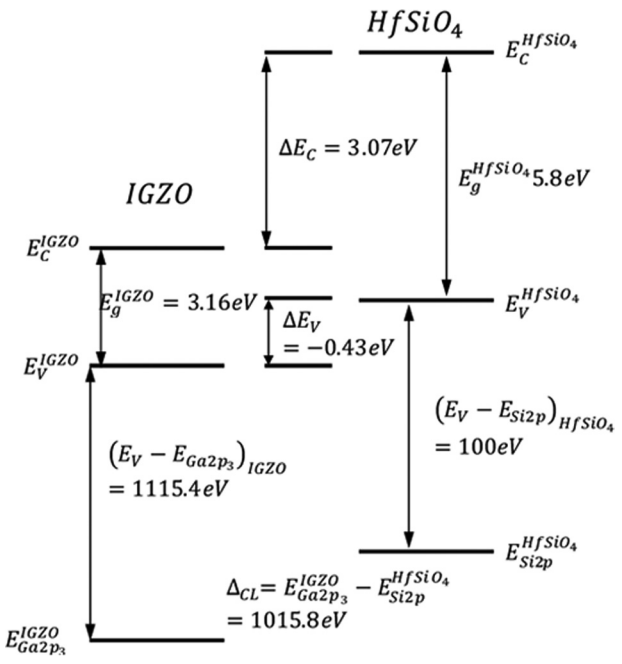

FIG. 18. Band diagrams for $HfSiO_4$/IGZO heterostructure vacuum samples (after Ref. 206).

like this and others such as the deposition technique for dielectric deposition which can affect stoichiometry or density of the films could be a reason for the spread in band offsets reported for dielectric/oxide interfaces in the literature.

2. $ZrSiO_4$

Zirconium silicate, $ZrSiO_4$, is an attractive candidate gate dielectric due to its stability and large bandgap of ~6.5 eV.[194–196] It is strongly corrosion-resistant and has a very high decomposition temperature (>1670 °C). It has a dielectric constant around 15 and has been established as a thermodynamically stable candidate for future CMOS devices in Si technology.[197] The fact that it is well-characterized makes it an attractive possibility for gates on IGZO TFTs. However, little is known about its band offsets with IGZO.

Figure 19 shows the detailed band diagram of the $ZrSiO_x$/IGZO heterostructure for the samples kept in a vacuum. Once again, the data show that this system has a staggered, type II alignment, with a small valence band offset of −0.12 eV ± 0.02 eV for samples in which all the layers were kept in a vacuum or −0.05 eV for samples exposed to atmosphere prior to the measurement. The respective conduction band offsets are then 2.86 eV for the vacuum samples and 2.93 eV for the vented samples. The conclusion of this result is that the $ZrSiO_x$/IGZO heterostructure is not a candidate as a gate for TFTs because we need positive offsets in both valence and conduction bands. The $ZrSiO_x$ might still have application as a passivation layer on IGZO-based devices, which suffer from bias-stress instabilities during atmospheric exposure.

3. $LaAlO_3$

Figure 20 shows the band diagram of the Lanthanum Aluminum Oxide (LAO) $LaAlO_3$/InGaZnO heterostructure. Our data show that this is a nested, type I alignment, with a

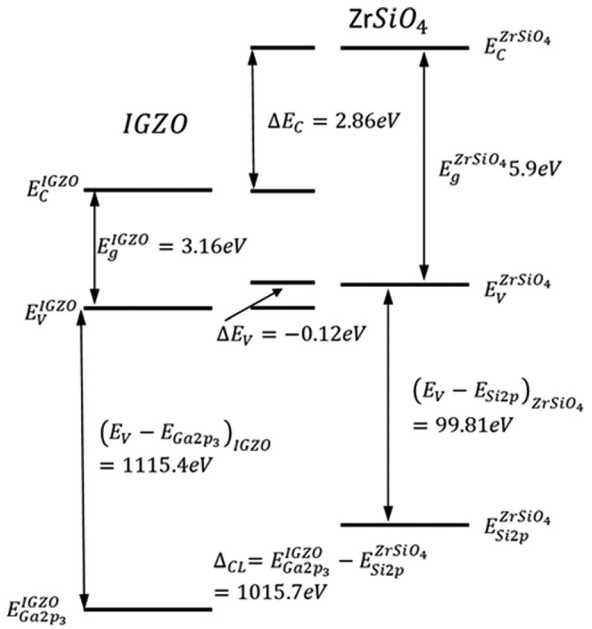

FIG. 19. Band diagrams for $ZrSiO_x$/IGZO heterostructure vacuum samples (after Ref. 116).

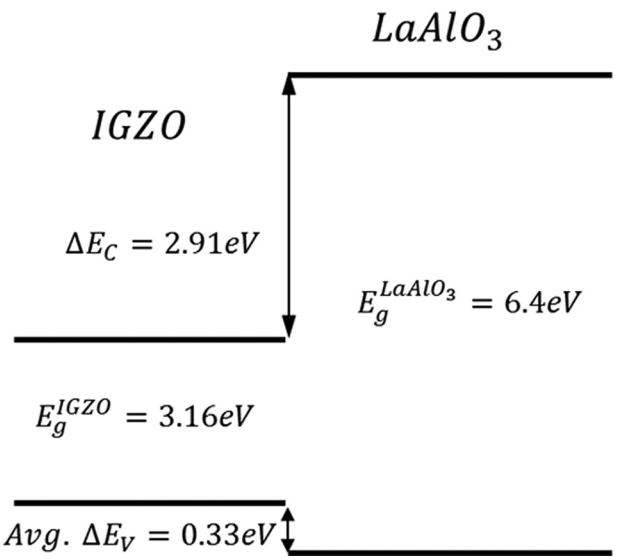

FIG. 20. Band diagrams for the $LaAlO_3$/IGZO heterostructure (after Ref. 117).

valence band offset of 0.33 eV and the conduction band offset is then 2.91 eV. The LAO is therefore a good choice as a gate dielectric on n-channel IGZO TFTs. If one could achieve p-type doping in this material, the valence band offset would not be sufficient to achieve good carrier confinement in such p-channel devices. It is worth considering one of the key potential applications for IGZO-based TFTs, namely, their use as switches or drivers in Active Matrix Liquid Crystal Display (AMLCD) panels or Active Matrix Organic Light Emitting Diode (AMOLED) screens. In these cases, the TFTs are under negative bias in the off-state most of the time but are illuminated from the backlit configuration of the LCD or the light from the organic Light Emitting Diodes (LEDs) in the AMOLED screens.[31] Thus, in these applications, there is still a requirement for minimizing injection of photo-excited holes from the channel into gate to avoid device instability and this demands a high valence band offset. The derived ΔE_v of 0.33 is larger or comparable to those of HfO_2 (0.38 eV), HfTiO (0.32 eV), ZrO_2 (0 eV), and Y_2O_3 (0.44 eV) but much less than that of SiO_2 on IGZO.

The LAO also appears to have a high thermodynamic stability on IGZO, which means that it could also be a good choice as a surface passivation layer to prevent surface conductivity changes upon exposure to hydrogen-containing ambients.[54] During examinations of gate-bias stability of unpassivated a-IGZO TFTs when the channel layer was exposed to hydrogen, oxygen, air, or vacuum at room temperature during measurements, the threshold voltage shift under gate-bias stress was faster in hydrogen than in oxygen and vacuum.[54] Under vacuum and hydrogen ambients, the threshold voltages showed a negative shift and the drain current increased in the typical transfer curves, while the trend was opposite under oxygen. This shows the need for careful passivation of the channel in these TFTs. It is clearly possible to choose dielectrics which will provide both good carrier confinement and low operating voltage operation and provide adequate surface passivation of IGZO TFTs using SiO_2

or LAO. LAO is certainly a suitable gate dielectric for the n-type IGZO in DC applications because of the large conduction band offset.

4. Sc_2O_3

The Sc_2O_3/IGZO heterojunction was found to have a type II alignment of band offsets with a valence band offset of ~1.67 eV ± 0.16 eV and a conduction band offset determined to be 4.07 eV from XPS measurements. This is shown in Figure 21. Thus, Sc_2O_3 would be an effective barrier for electrons but not for holes on IGZO and would not be a good choice as a gate dielectric on transparent TFTs based on IGZO.[203–206] However, it still may have application as a passivation layer to prevent exposure of the IGZO surface to hydrogen and oxygen.

5. HfO_2

A bandgap of ~5.8 eV was determined for HfO_2. These results agree with the previous reports of sputtered HfO_2 with the value ranging from 5.5–5.8 eV[200,201] but lower than some reports (6.07 eV).[207] A survey of the literature finds these types of variation in reported oxide bandgaps to be common and most likely due to variations in stoichiometry and defect concentration. The HfO_2/IGZO heterojunction is found to have a straddling gap alignment of band offsets with a valence band offset of ~0.38 eV ± 0.03 eV and a conduction band offset was determined to be 2.26 eV determined from XPS measurements.

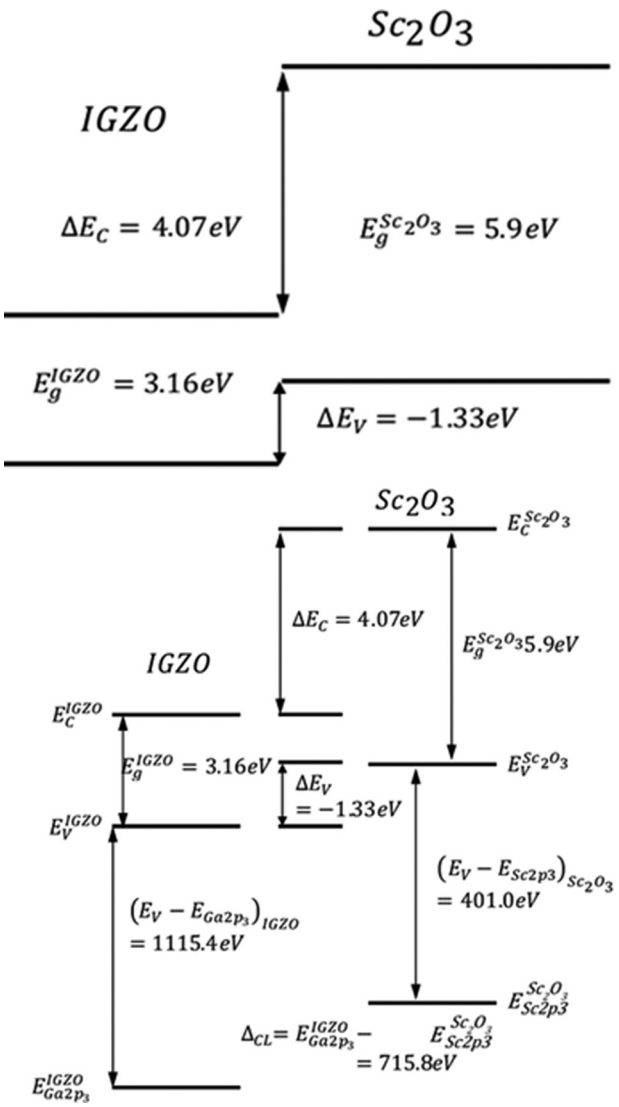

FIG. 21. Summary (top) and detailed (bottom) band diagrams for Sc_2O_3/IGZO (after Ref. 114).

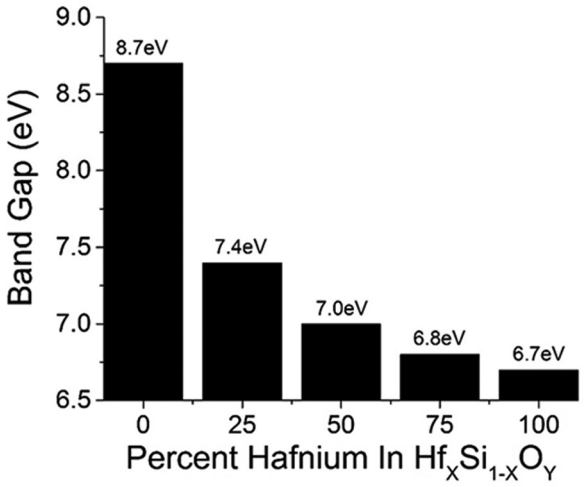

FIG. 22. Bandgaps of $Hf_xSi_{1-x}O_y$ as a function of composition (after Ref. 206).

6. $Hf_xSi_{1-x}O_y$

Figure 22 shows the bandgaps of ALD deposited $Hf_xSi_{1-x}O_y$ as a function of composition and Figure 23 shows a summary of band diagrams of the $Hf_xSi_{1-x}O_y$ /InGaZnO heterostructure. Our data on films deposited by Atomic Layer Deposition (ALD) show that this is a nested, type I alignment, with a valence band offset ranging from 1.73 eV for SiO_2 to 0.52 eV for HfO_2. In this case, a positive offset indicates that the IGZO valence band lies closer to the vacuum level than

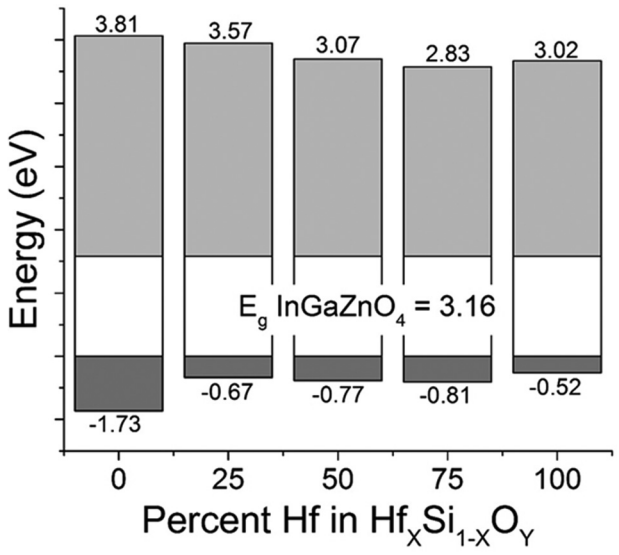

FIG. 23. Conduction and valence band offsets as a function of percent Hf in $Hf_xSi_{1-x}O_y$. (after Ref. 206).

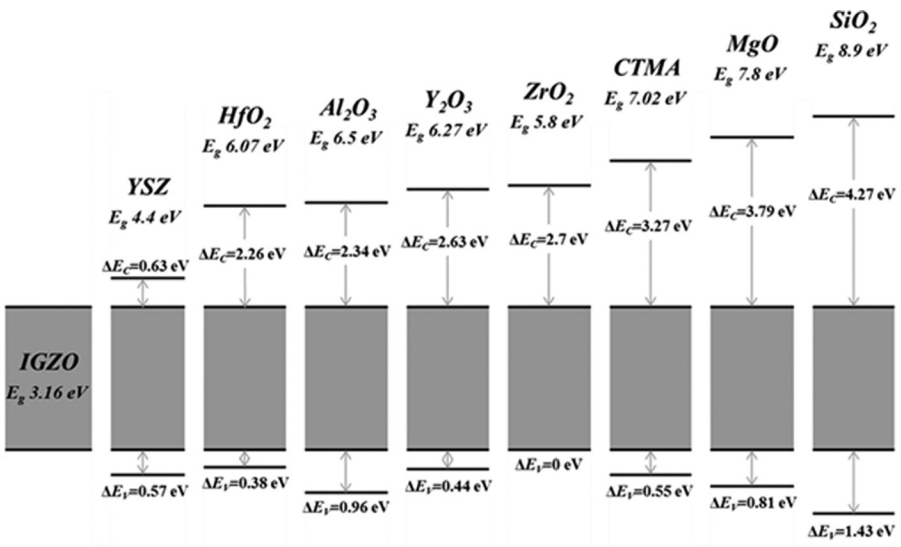

FIG. 24. Summary of reported band offsets for dielectrics on a-IGZO.

that of the dielectric. The conduction band offsets are then 3.81 eV for SiO_2, 3.02 eV for HfO_2, and range from 2.83–3.57 eV for $Hf_xSi_{1-x}O_4$ with x = 0.25 to 0.75 using the relationship: $\Delta E_C = E_g^{Dielectric} - E_g^{IGZO} - \Delta E_V$. The $Hf_xSi_{1-x}O_y$/a-IGZO heterostructure therefore forms a straddling (type I) nested band alignment across the entire composition range of Hf. The VBM data follow a linear relationship, as expected for a mixing rule, but diverge at pure SiO_2.

The comparison of ALD deposited dielectrics with previous results from PECVD or sputtered films allows us to identify mechanisms that can lead to differences in band alignment, including stoichiometry and contamination of the dielectric and the resulting determination of the bandgap, surface disorder effects on the oxide, and surface history. Figure 24 shows a summary of reported band offsets for dielectrics on a-IGZO.

IV. DISCUSSION

We examined the band offsets of a variety of materials under different processing conditions and determined some potential causes for shifts in these data based on support from the literature. The errors introduced by the measurement techniques (of order 0.1 eV) themselves are relatively small compared to the variations reported by various groups for nominally the same interface, which can be 0.5 eV. One thing that is needed in future studies of IGZO/dielectrics is a more standard approach to detailing how the materials was deposited, resultant properties of the IGZO, core level-VBM values,[211–217] and issues with bandgap determination of the dielectric and any charge compensation methods used during analysis.

It is useful to compare experimental values to the predicted offsets in order to gain a deeper understanding of the differences we have measured and determine the magnitude of the assumed effect. To determine the expected offsets for each material, a freeware modeling program from Boise State University was used.[218,219] The program uses a modular approach to solve the 1-D Poisson equation for each material independently and calculate the charge, electric field, potential, and energy of the multilayer structure. Details are explained by Southwick *et al.*[218,219] The inputs we used in this bandgap program are shown in Table III, along with the references for the input values. This at least provides a reference point in predicting band offsets and a comparison to experimental values. It also points out the future developments needed in the models to predict the offsets because they typically cannot simulate effects like interface states, defects, and polarization. Mutch *et al.*[220] give an example of where this program is used with a previously determined photoemission derived band alignment as an actual input.

The predicted (red dashed lines) and measured (black lines) band offsets are shown in Figure 25. All of the measured offsets are shifted upwards compared to the modeled data. This result is not unexpected since the model assumes ideal surfaces and interfaces which is not the case for real-world samples (i.e., contamination, surface roughness, and dangling bonds). Table IV gives a summary of the offset values and the delta (actual–predicted) between them. If the

TABLE III. Summary of values used for input into the model described by Southwick *et al.*[218,219]

Dielectric	Bandgap (eV)	Electron affinity (eV)	Dielectric constant
HfO_2	6[a]	2.4[a]	25[b]
$HfSiO_4$	6.5[a]	2[a]	11[b]
$LaAlO_3$	5.6[a]	2.5[a]	30[b]
Sc_2O_3	6.3[c]	1.9[a]	14[c]
SiO_2	9[a]	0.9[a]	3.9[b]
$ZrSiO_4$	6.5[a]	2.4[a]	15[d]
Semiconductor			
$InGaZnO_4$	3.2[e]	4.16[f]	16[e]
Intrinsic carrier concentration = 10^8 cm^{-3} [g]			
Dopant carrier concentration = 3×10^{19} cm^{-3} [f]			

[a]Ref. 243.
[b]Ref. 244.
[c]Ref. 245.
[d]Ref. 246.
[e]Ref. 247.
[f]Ref. 248.
[g]Ref. 249.

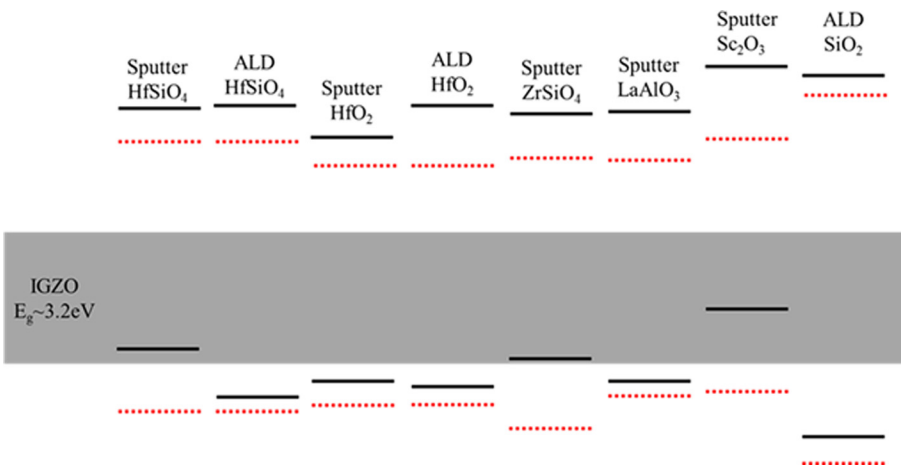

FIG. 25. Graphical representation of predicted and actual band offsets of various dielectrics on IGZO.

data are divided into ALD versus sputtered films, it is seen that there is a measurable difference between the two. The most dramatic difference is seen in the ΔEv values where the average difference for the sputter samples is ∼−1.19 eV and the average for the ALD samples is ∼−0.48 eV.

During film deposition, a transition region is typically formed that consists of various defects that can result in the formation of dipoles. The origin of the dipole can take many forms such as lattice strain inducing polarization at the interface.[218,219] Such lattice strain has been shown to differ depending on the deposition method.[221–223] Balaz *et al.*[224] showed that dipoles due to highly mismatched $BaTiO_3$/$SrTiO_3$ heterostructures can produce polarization values of 43 $\mu C/cm^2$. However, after getting similar tensile stress values for both sputtered films of $ZrSiO_4$ and $LaAlO_3$, it does not appear that strain induced polarization is the source of the large differences seen. Since strain generated variations are largely due to changes in crystal symmetry, this effect is not present for the amorphous materials used here.

Another potential origin for shifting the offsets could be a change in bonding or stoichiometry of the dielectric. When investigating this effect, it would be useful to examine the $HfSiO_4$ films deposited by each method (ALD and sputter) because of the large ΔEv. With a difference of ∼1.14 eV between the actual valence band offsets between the two methods, one would expect significant changes in bonding or stoichiometry if this is the true origin. When comparing the Hf:Si ratios, it is found that they are essentially 1:1 for both. While the Hf:Si ratios appear to be correct, these elements could possibly not be fully oxidized or could even form silicide bonds (Hf-Si bonds). The Hf-Si bonds shift the Hf 4f peaks to a higher binding energy of ∼1 eV.[225] Elemental silicon and hafnium peaks appear at approximately 4 eV lower binding energies than the oxide.[226] A further analysis of the XPS data is shown in Figure 26 and shows no presence of silicide formation or metallic hafnium or silicon, indicating that the Hf and Si atoms have formed bonds solely with oxygen atoms.

A number of papers have reported on the presence of interface defects, such as oxygen or metal atom vacancies, and the effect that they can have on the band offsets of materials.[227–234] The magnitude of the defects as modeled by Zur and McGill[228] was found to be on the order of 10^{12} e^-/cm^2 to produce significant shifts. Defect densities of this magnitude will produce a shift up or down, depending on the sign of the charge, of ∼0.3 eV. In order to induce a shift in the valence band towards the vacuum level, a negative charge must be present and was confirmed using the Boise State Band Model Program. The program has the ability to insert a fixed charge anywhere within the dielectric. In a recent paper by Dong and Shi[229] it was shown that the most stable defects consist of Hf and Si vacancies and O interstitial defects, all of which result in a negative fixed charge.

It is possible to use the O1s peak to resolve the number of oxygen defects from lattice oxygen[137,232,234] by deconvolving the O1s peak into three components consisting of low, mid, and high energy regions. The low binding energy component is the well-defined position corresponding to lattice oxygen that is bound to the metal atoms. The mid-binding energy peak is assigned to oxygen defects. Figure 27

TABLE IV. Predicted and actual band offsets with calculated differences. The predicted values come from the model described by Southwick *et al.*[218,219]

Material	Predicted E_V	Predicted E_C	Actual E_V	Actual E_C	Delta E_V	Delta E_C
ALD SiO_2	2.4	3.3	1.73	3.81	−0.67	0.51
ALD HfO_2	0.95	1.56	0.52	3.02	−0.43	1.46
ALD $HfSiO_4$	1.1	2.2	0.77	3.07	−0.33	0.87
Sputter HfO_2	0.95	1.56	0.38	2.26	−0.57	0.7
Sputter $HfSiO_4$	1.1	2.2	−0.37	3.01	−1.47	0.81
Sputter $LaAlO_3$	0.7	1.7	0.33	2.91	−0.37	1.21
Sputter $ZrSiO_4$	1.49	1.8	−0.12	2.86	−1.61	1.06
Sputter Sc_2O_3	0.6	2.2	−1.33	4.07	−1.93	1.87

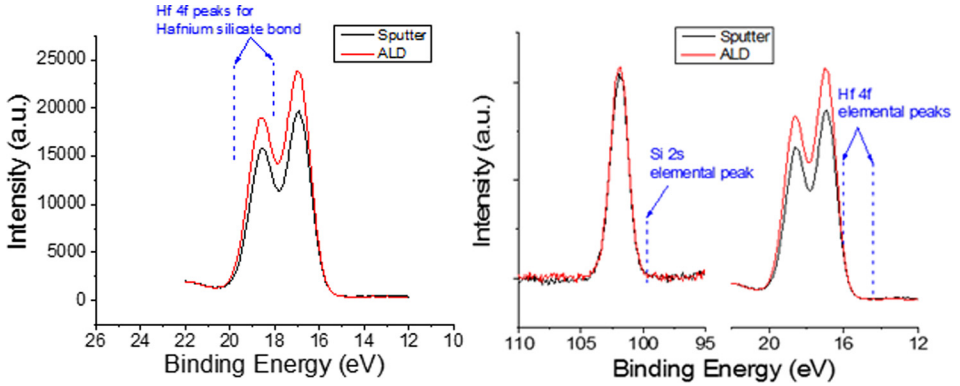

FIG. 26. XPS spectra from sputtered and ALD $HfSiO_4$ indicating required binding energy shifts for Hf-Si bonds and elemental Hf and Si.

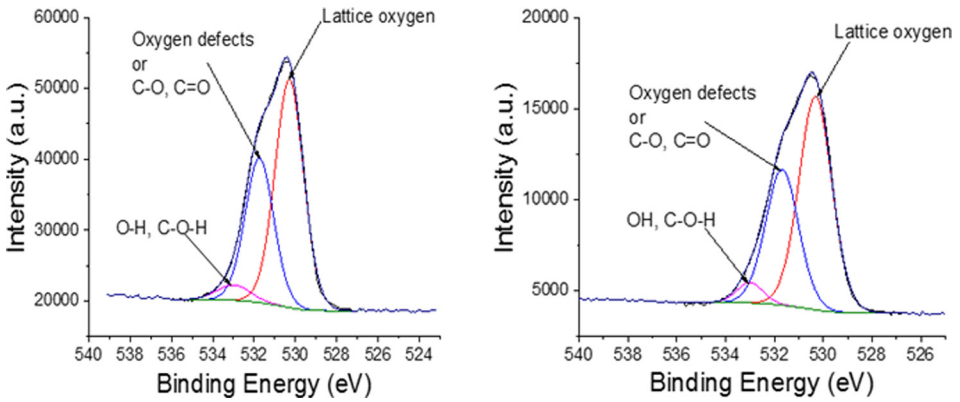

FIG. 27. XPS spectra of O1s peak from sputtered (left) and ALD (right) $HfSiO_4$ showing components assigned to oxygen compounds/defects.

shows the O1s spectra from sputtered (left) and ALD (right) $HfSiO_4$ with the three synthetic components that produce the overall peak shape. The spectra from both samples have similar shapes and almost identical areas under each component curve. Using the interpretation from Rahimnejad[232] and Rumaiz,[234] one would conclude that the two materials have similar oxygen defects. The matter is further complicated by the presence of surface carbon, which is not discussed in these articles. The traditional components of the O1s spectrum on metal oxides consist of three peaks of 530–531 eV for lattice oxygen, 531–533 eV for C-O and C=O, and 533–534 eV for O-H and C-O-H groups[235–238] and are also shown in Figure 27. The mid-binding energy component for C-O/C=O lies at the same energy assigned to the oxygen defects and separating the contributions of each will be difficult to determine. While the defects are most certainly present, it is difficult to determine the magnitude of the effect using spectra with high carbon backgrounds.

Another indicator of defects/vacancies is present in the valence band spectra. When comparing the density of states for pure $HfSiO_4$ and the most likely defect states from the work by Dong and Shi,[229] it is demonstrated that these can produce significant shifts in the valence and conduction bands, shown in Figure 28. Vacancies in $HfSiO_4$ tend to push the VBM to higher energies, especially for Hf vacancies and O interstitials. In addition, the CBM can be lowered for both the metal vacancies, which reduces the bandgap dramatically. Applying this to the ALD and sputtered $HfSiO_4$ data, shown in Figure 29, we see a substantial shift of the VBM for the sputtered material to higher energies by over 1 eV. In addition, the onset of the valence band is not as distinct in the sputtered material, which indicates greater tailing effects due to defects (shaded region in Figure 29). The modeled density of states for pure $HfSiO_4$ shows a VBM at ∼3 eV and a bandgap of ∼7 eV, which matches the ALD material almost perfectly. The sputtered material has a VBM of ∼2.2 eV, which could indicate a mixture of Hf vacancies

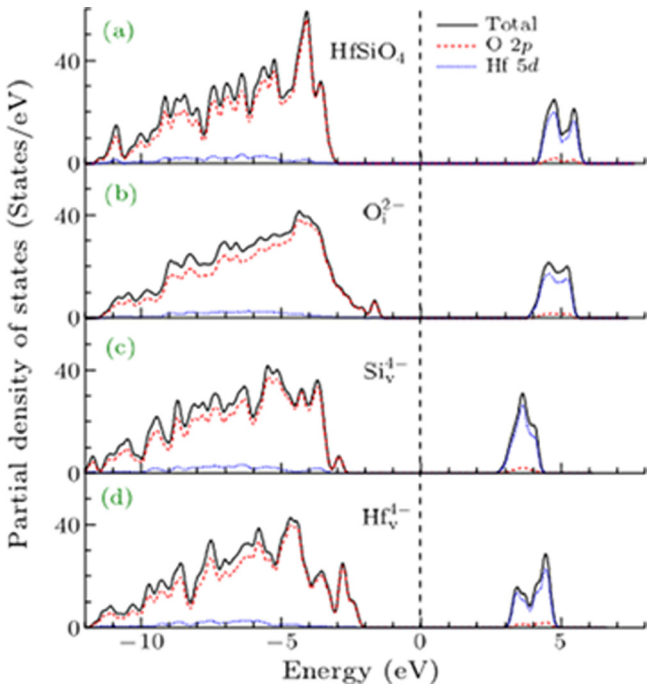

FIG. 28. The density of states of (a) pure $HfSiO_4$, (b) containing O_i^{2-}, (c) containing Si_V^{4-}, and (d) containing Hf_V^{4-} (after Ref. 225).

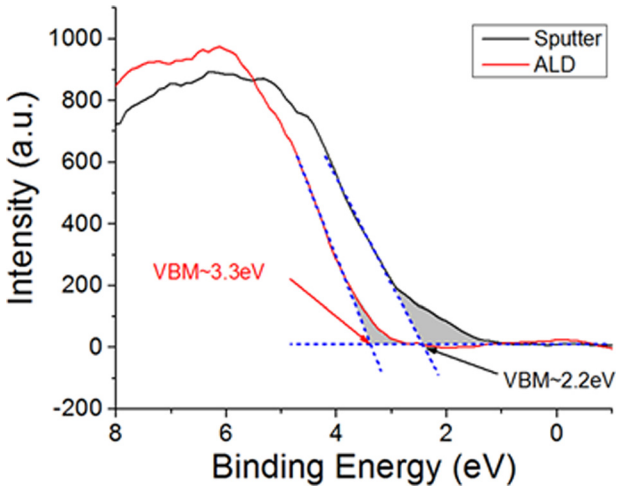

FIG. 29. Comparison of valence band spectra for sputtered and ALD $HfSiO_4$. Shaded regions indicate tailing effects due to defects.

and O interstitials. However, with a measured bandgap of 6 eV, this matches the signature of O interstitials more than Hf vacancies, which will reduce the bandgap in the 5 eV range.

The data obtained from XPS can be used to determine the concentration of atoms on the near surface of materials. It was already shown that the stoichiometry of the film does not fully explain differences in the band offsets that have been measured. While all of the ALD data did not indicate the presence of any metal contaminants, most of the sputter data showed the existence of considerable concentrations of Ti, Cr, Cu, and Fe, sometimes as high as 9 atomic percent total. Taking the total concentration of contaminants and plotting it against ΔEv (measured – predicted), a clear pattern is observed and shown in Figure 30. The literature shows that energy band alignment variations of sometimes more than 1 eV depending on interface preparation can be obtained,[212–215,239–242] due to the presence of high defect concentrations in the materials and on a cation effect that will increase the VBM of that material.[117] The oxides of Ti, Cr, Cu, and Fe have much lower bandgaps (~1.5–3.4 eV) and thus contribute to a lowering of

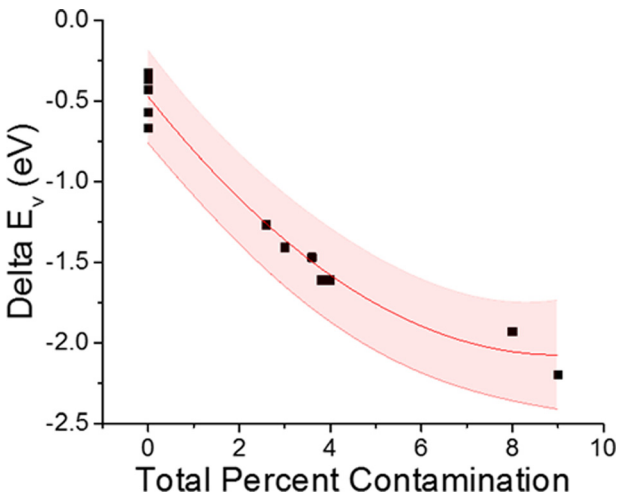

FIG. 30. Difference of actual band offset to predicted offset versus total percent contamination in the film.

the average gap of the films.[143] Thus, sputtered films containing metallic contaminants and interfacial disorder due to the sputter-induced damage, which leads to Fermi level pinning effects, are less likely to be accurate than a more controlled process such as ALD with a more abrupt interface and far fewer expected defects. We measured stress in our films on calibration pieces using the wafer bow technique using a Tencor long scan profilometer. The film stress was estimated from Stoney's equation.[161] The stresses in all films were small, <80 MPa in all cases.

In a similar vein, for SiO_2 deposited by PECVD, Douglas *et al.*[180] reported a band offset of 1.43 eV on IGZO compared to 1.73 eV for ALD deposition. In that case, at least part of the difference may result from the hydrogen incorporated in the PECVD oxide. The net effect of H_2 is to lower the valence band edge, by about 0.04% for each percent hydrogen.[217] The observed valence band offset difference between PECVD and ALD SiO_2 on IGZO would then indicate ~7.5% difference in hydrogen content between the two types of film using this model, which is consistent with the experimental data.

Similar to measuring the valence band offsets, measurement of the bandgap can be quite difficult to extract precise values, specifically using REELS, which can lead to large variations seen in reported ΔEc values. For sputter deposited $HfSiO_4$ on IGZO, we measured bandgaps of 5.8–5.9 eV and valence band offsets of −0.27 to −0.43 eV,[188] depending on whether the samples were exposed to atmosphere prior to deposition of the dielectric. This result is much different than the bandgap obtained for ALD $HfSiO_4$ of 7 eV, with a valence band offset of 0.77 eV on IGZO. One issue with determining the bandgap with REELS is that there is some ambiguity in the measurement where some studies employ a horizontal fit to the curve at the lowest intensity, but this is only valid if the curve is flat-bottomed.

Contamination in the films from water and carbon can lead to high backgrounds, which creates a shoulder where there should be a flat region. Because the technique is somewhat surface sensitive at 1 kV, dangling bonds from vacancies can also lead to raised backgrounds or even "smear" the energy distribution.[235,236] If the data have no flat region, the fit is usually made to the lower slope region, but this often gives an artificially large bandgap. For example, as shown in Figure 9 with sputter deposited $HfSiO_4$ on IGZO,[188,206] using both methods with a 95% confidence interval in the lower slope region data produces a bandgap between 7.1 and 7.6 eV, which is too high, while the horizontal fit gives between 5.7 and 5.9 eV. The large difference in these values will artificially raise ΔEc, leading to incorrect assumptions on its carrier confinement capability.

It should be pointed out that these types of experiments can provide powerful guidance in understanding the behavior and reliability of things like metal interconnects.[220] Mutch *et al.*[220] measured the band alignment single and dual damascene low-k/Cu interconnect structures using specifically report combined XPS and REELS measurements. They measured the valence and conduction band offsets present at the interface between a-SiN(C):H dielectric Copper Clad Laminates (CCLs) and low-k a-SiOC:H interlevel dielectrics. They added electron

paramagnetic resonance (EPR) and electrically detected magnetic resonance (EDMR) measurements to identify mid-gap carbon and silicon dangling bond defects in the low-k interlevel dielectric and Cu capping layer playing a role in electronic transport in these materials.[220] In other words, these combined band and defect state measurements can explain and predict some of the observed reliability issues reported for technologically important systems like low-k/Cu interconnects.

Uncertainties in reported binding energy peak positions can arise from three main sources;

(1) Improper calibration of the binding energy scale.
(2) Missing components or improper constraints associated with peak fitting.
(3) Charging/differential charging.

The XPS spectrometer we used was calibrated using a polycrystalline Au foil. The peak position and Fermi-edge inflection point for the Au f7/2 peak were determined to be 84.006 ± 0.02 and 0.006 ± 0.02 eV, respectively. The binding energy range of 0–100 eV is accurate on an absolute scale within 0.02–0.03 eV. To ensure precision and accuracy during peak analysis, we used only peaks with high intensities to increase the signal to noise ratio. Peaks were deconvoluted using NIST assigned constraints such as peak ratios and FWHM and included component peaks for the element as well as oxides. Sample charging is not an issue when determining band offsets since we only need peak deltas, which will shift all binding energies by the same amount. However, differential charging of multilayer samples will shift peaks by different amounts and could potentially be a large source of error. Based on our results, we did not see any effects of differential charging and will assume it does not play a role in band offsets on IGZO. Based on the described methods, we have determined that peak position error is ±0.1 eV.

For measurements defined from linear regression analysis, the measurement error can be much larger. We quantified the uncertainty of these measurements by using a 95% confidence interval to the regression analysis. When determining the valence band maximum, the leading edge of the valence band was fit using the 95% CI to the flat energy distribution, with an error of ±0.2 eV. The same procedure was applied to measuring the bandgap by UV/Vis and resulted in an error of ±0.2 eV. By far the largest source of error was determining the bandgap via REELS. The onset of energy loss was analyzed by taking the upper and lower bounds of the confidence intervals and finding their intersection with the horizontal line representing the background level with an associated error was ±0.5 eV.

Figure 31 indicates the worst case scenario where all of the errors are maximized in opposite directions. The shaded regions indicate the measurement error around a center point in blue. The cumulative for each band (Ec or Ev) is shown outside of each shaded region. The total impact to the valence or conduction band offset between IGZO and a dielectric is indicated by the arrows. The result is a maximum error of ∼0.6 eV for the VBO and ∼1.3 eV for the CBO.

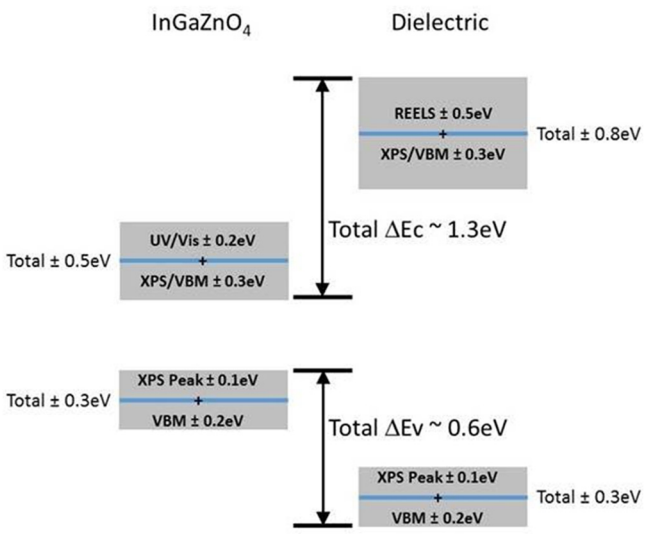

FIG. 31. Analysis of maximum values of sources of error in measurement of band offsets on a-IGZO.

All of these results point out pitfalls in determining band offsets in oxide systems where the role of dielectric stoichiometry and purity, interfacial disorder, oxide surface polarity, and role of atmospheric exposure prior to dielectric deposition may all influence the resulting band offsets. Through this systematic study, we have been able to determine some of the mechanisms, and their magnitudes, that can produce shifts to band offsets on $InGaZnO_4$, which is shown in Table V. It is suggested that controlled, low damage processes such as ALD are less likely to include such effects. Finally, Figure 32 provides a summary of all reported offsets of dielectrics on IGZO. The data from this work are shown in red for ALD and blue for sputtered material. All other values from the literature are shown in gray.

Finally, although we have given a discussion earlier of charging effects, it is worth repeating that this has generally not been a focus of previous studies of IGZO/dielectric band offset measurements beyond using the standard electron flood gun and the calibration to the adventitious carbon peak. In our experiments, we have not observed clear signs of differential charging between the dielectric and the IGZO but that that does not preclude this effect being present in future investigations of other dielectrics relative thicknesses of

TABLE V. Mechanisms contributing to valence band offsets for the studied dielectrics on $InGaZnO_4$ and their magnitudes. Differences in bandgaps of the dielectrics due to stoichiometric differences affect the conduction band offset.

Mechanism	Reported/observed magnitude (eV)	% of IGZO bandgap	Effect
Metal contamination	0.3–1	9–30	Strong
Inferface disorder/vacancies	0.3–1	9–30	Strong
Dielectric composition	0.2–0.5	6–15	Strong
Carbon contamination	0.1–0.2	3–6	Moderate
Annealing	<0.1	<3	Weak
Stress/strain	<0.1	<3	Weak
Surface termination	<0.1	<3	Weak
Differential Charging	<0.1	<3	Weak

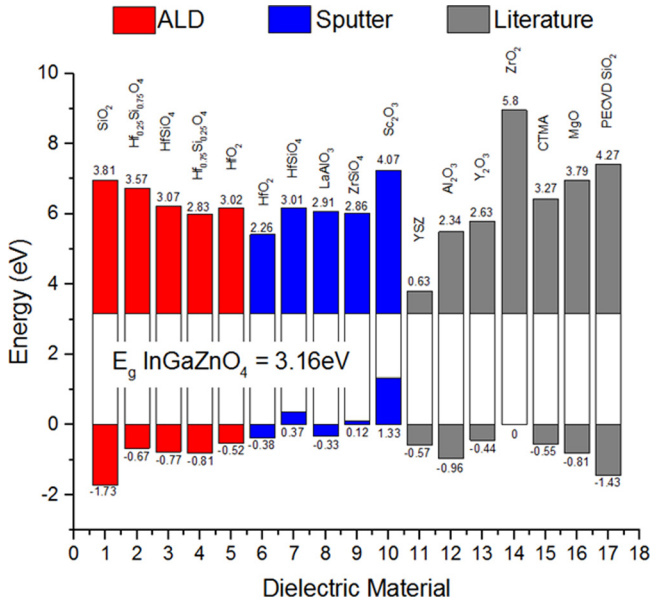

FIG. 32. Summary of conduction and valence band offsets for dielectrics on a-IGZO.

dielectric and semiconductor or different conductivity levels in the IGZO.

V. SUMMARY AND CONCLUSIONS

A review of band offsets for gate dielectric materials on a-IGZO has been given. The factors that influence the variability reported in the literature for both valence and conduction band offsets were discussed and their relative magnitudes quantified. Some of these effects include metal contamination, interface disorder, dielectric composition, carbon/hydrogen contamination, annealing, stress/strain, and surface termination. In some cases, these result in differences in the bandgap of the dielectric and thus affect the conduction band offset since the valence band offset is directly measured but can also be affected by most of these same issues. The most promising gate dielectrics are SiO_2, Al_2O_3, $HfSiO_4$, and $LaAlO_3$. There are issues with the degradation of the surface of IGZO during exposure to plasmas involving hydrogen, as we have seen significant loss of oxygen from the surface during PECVD deposition of SiNx. Some key recommendations for future directions are as follows:

(i) A focus on ALD dielectric films for IGZO which provide a more controlled, lower damage process than sputtering or PECVD and are less likely to include effects like surface disorder, metal or carbon contamination, and possible film stress-induced shifts. This is of particular interest in the bandgap determination by REELS, where the spectrum fitting choice can be affected by high energy spectral shoulders created by defects or contamination. Due to the extremely low deposition rate, some sputtered dielectrics were observed to incorporate re-sputtered material from tool components (mostly Ti, Cr, Cu, and Fe) that can lead to VBM shift due to the cation effect and also lower the effective bandgap.

(ii) Continued systematic studies on the role of contamination by air exposure, which also leads to carbon and hydrocarbon layers at the interface between the IGZO and the dielectric and the effect on band offsets.

(iii) The role of thermal annealing and overall thermal budget in interface stability and band offsets for specific dielectrics on IGZO.

(iv) Continued monitoring for the presence of differential charging. This may become more significant in conditions where very conducting IGZO is used in conjunction with very large gap dielectrics or with multilayer dielectrics that have differences in conductivity.

(v) Examination of stacked dielectrics to optimize both interfacial stability and effective dielectric constant.

(vi) Examination of other members of the Lanthanate family that combine high –K and good environmental stability.

(vii) Standardizing details of how the experimental materials were deposited, the properties of the IGZO, core level-VBM values, and issues with bandgap determination of the dielectric and any charge compensation methods used during analysis.

(viii) Continued refinement of models to predict VBO and CBO values that incorporate the effects of interfacial disorder and contamination.

ACKNOWLEDGMENTS

The work at UF was partially supported by NSF Grant No. 1159682. The project or effort depicted was also sponsored by the Department of the Defense, Defense Threat Reduction Agency, HDTRA1-17-1-011, monitored by Jacob Calkins. The content of the information does not necessarily reflect the position or the policy of the federal government, and no official endorsement should be inferred.

[1]R. L. Hoffman, B. J. Norris, and J. F. Wager, Appl. Phys. Lett. **82**, 733 (2003).
[2]S. Masuda, K. Kitamura, Y. Okumura, S. Miyatake, H. Tabata, and T. Kawai, J. Appl. Phys. **93**, 1624 (2003).
[3]P. F. Carcia, R. S. McLean, M. H. Reilly, and G. Nunes, Appl. Phys. Lett. **82**, 1117 (2003).
[4]Jun-Hyun Park, Hyun-Kwang Jung, Sungchul Kim, Sangwon Lee, Dong Myong Kim, and Dae Hwan Kim, IEEE Trans. Electron Dev. **58**, 2796 (2011).
[5]J. K. Jeong, Semicond. Sci. Technol. **26**, 034008 (2011).
[6]J. Nishii, F. M. Hossain, S. Takagi, T. Aita, K. Saikusa, Y. Ohmaki, I. Ohkubo, S. Kishimoto, A. Ohtomo, T. Fukumura, F. Matsukura, Y. Ohno, H. Koinuma, H. Ohno, and M. Kawasaki, Jpn. J. Appl. Phys., Part 2 **42**, L347 (2003).
[7]M. J. Gadre and T. L. Alford, Appl. Phys. Lett. **99**, 051901 (2011).
[8]E. Fortunato, A. Pimentel, L. Pereira, A. Goncalves, G. Lavareda, H. Aguas, I. Ferreira, C. N. Carvalho, and R. Martins, J. Non-Cryst. Solids **338–340**, 806 (2004).
[9]M.-J. Choi, M.-H. Kim, and D.-K. Choi, Appl. Phys. Lett. **107**, 053501 (2015).
[10]E. M. C. Fortunato, P. M. C. Barquinha, A. C. M. B. G. Pimentel, A. M. F. Goncalves, A. J. S. Marques, L. M. N. Pereira, and R. F. P. Martins, Adv. Mater. **17**, 590 (2005).
[11]R. A. Street, Adv. Mater. **21**, 2007 (2009).
[12]J. C. Knights, G. Lucovsky, and R. J. Nemanich, Philos. Mag. B **37**, 467 (1978).
[13]G. Lucovsky, R. J. Nemanich, and J. C. Knights, Phys. Rev. B **19**, 2064 (1979).

[14]R. A. Street, *Hydrogenated Amorphous Silicon* (Cambridge University Press, Oxford, UK, 2005).
[15]S. D. Brotherton, Semicond. Sci. Technol. **10**, 721 (1995).
[16]J. S. Custer, M. O. Thompson, D. C. Jacobson, J. M. Poate, S. Roorda, W. Sinke, and F. Spaepen, Appl. Phys. Lett. **64**, 437 (1994).
[17]S. Adachi and H. Mori, Phys. Rev. B **62**, 10158 (2000).
[18]J. E. Anthony, A. Facchetti, M. Heeney, S. R. Marder, and X. W. Zhan, Adv. Mater. **22**, 3876 (2010).
[19]H. Sirringhaus, Adv. Mater. **21**, 3859 (2009).
[20]T. Kamiya, K. Nomura, and H. Hosono, Sci. Technol. Adv. Mater.**11**, 44305 (2010).
[21]P. Gorrn, M. Sander, J. Meyer, M. Kroger, E. Becker, H. H. Johannes, W. Kowalsky, and T. Riedl, Adv. Mater. **18**, 738 (2006).
[22]W. B. Jackson, R. L. Hoffman, and G. S. Herman, Appl. Phys. Lett. **87**, 193503 (2005).
[23]E. M. C. Fortunato, P. M. C. Barquinha, and R. F. P. Martins, Adv. Mater. **24**, 2945 (2012).
[24]J. Park, W. Maeng, H. Kim, and J. Park, Thin Solid Films **520**, 1679 (2011).
[25]T. Kamiya, K. Nomura, and H. Hosono, Sci. Technol. Adv. Mater. **11**, 1 (2010).
[26]J. Y. Kwon, D. J. Lee, and K. B. Kim, Electron. Mater. Lett. **7**, 1 (2011).
[27]T. C. Fung, T. Chuang, K. Nomura, H. P. Shieh, H. Hosono, and J. Kanicki, J. Inf. Disp. **9**, 21 (2008).
[28]Binn Kim, Hyung Nyuck Cho, Woo Seok Choi, Seung-Hee Kuk, Yong Ho Jang, Juhn-Suk Yoo, Soo Young Yoon, Myungchul Jun, Yong-Kee Hwang, and Min-Koo Han, IEEE Electron Dev. Lett. **33**, 528–530 (2012).
[29]T. Y. Hsieh, T. C. Chang, T. C. Chen, M. Y. Tsai, Y. T. Chen, F. Y. Jian, Y. C. Chung, H. C. Ting, and C. Y. Chen, Appl. Phys. Lett. **99**, 022104 (2011).
[30]T. C. Chen, T. C. Chang, T. Y. Hsieh, M. Y. Tsai, C. T. Tsai, S. C. Chen, C. S. Lin, and F. Jian, Surf. Coat. Technol. **231**, 465 (2013).
[31]S. Park, E. N. Cho, and I. Yun, J. Soc. Inf. Disp. **21**, 333 (2013).
[32]J. Yao, N. Xu, S. Deng, J. Chen, J. She, H. D. Shieh, P. T. Liu, and Y. P. Huang, IEEE Trans. Electron Devices **58**, 1121 (2011).
[33]N. L. Dehuff, E. S. Kettenring, D. Hong, H. Q. Chiang, J. F. Wager, R. L. Hoffman, C. H. Park, and D. A. Keszler, J. Appl. Phys. **97**, 064505 (2005).
[34]B. Yaglioglu, H. Y. Yeom, R. Beresford, and D. C. Paine, Appl. Phys. Lett. **89**, 062103 (2006).
[35]E. Fortunato, P. Barquinha, A. Pimentel, L. Pereira, G. Goncalves, and R. Martins, Phys. Status Solidi RRL **1**, R34 (2007).
[36]L. Liang, J. Yu, M. Wang, and H. Cao, ECS Trans. **75**, 261 (2016).
[37]E. K.-H. Yu, S. Jun, D. H. Kim, and J. Kanicki, J. Appl. Phys. **116**, 154505 (2014).
[38]J. I. Song, J. S. Park, H. Kim, Y. W. Heo, J. H. Lee, J. J. Kim, G. M. Kim, and B. D. Choi, Appl. Phys. Lett. **90**, 022106 (2007).
[39]S. Lee, M. M. Billah, M. Mativenga, and J. Jang, ECS Trans. **75**, 201 (2016).
[40]N. Itagaki, T. Iwasaki, H. Kumomi, T. Den, K. Nomura, T. Kamiya, and H. Hosono, Phys. Status Solidi A **205**, 1915 (2008).
[41]T. Miyasako, M. Senoo, and E. Tokumitsu, Appl. Phys. Lett. **86**, 162902 (2005).
[42]K. Ide, K. Nomura, H. Hiramatsu, T. Kamiya, and H. Hosono, J. Appl. Phys. **111**, 073513 (2012).
[43]H. Q. Chiang, J. F. Wager, R. L. Hoffman, J. Jeong, and D. A. Keszler, Appl. Phys. Lett. **86**, 013503 (2005).
[44]P. Gorrn, P. Holzer, T. Riedl, W. Kowalsky, J. Wang, T. Weimann, P. Hinze, and S. Kipp, Appl. Phys. Lett. **90**, 063502 (2007).
[45]M. K. Jayaraj, K. J. Saji, K. Nomura, T. Kamiya, and H. Hosono, J. Vac. Sci. Technol. B **26**, 495 (2008).
[46]M. S. Grover, P. A. Hersh, H. Q. Chiang, E. S. Kettenring, J. F. Wager, and D. A. Keszler, J. Phys. D: Appl. Phys. **40**, 1335 (2007).
[47]K. J. Saji, M. K. Jayaraj, K. Nomura, T. Kamiya, and H. Hosono, J. Electrochem. Soc. **155**, H390 (2008).
[48]K. Nomura, H. Ohta, A. Takagi, T. Kamiya, M. Hirano, and H. Hosono, Nature **432**, 488 (2004).
[49]H. Yabuta, M. Sano, K. Abe, T. Aiba, T. Den, H. Kumomi, K. Nomura, T. Kamiya, and H. Hosono, Appl. Phys. Lett. **89**, 112123 (2006).
[50]T. Iwasaki, N. Itagaki, T. Den, H. Kumomi, K. Nomura, T. Kamiya, and H. Hosono, Appl. Phys. Lett. **90**, 242114 (2007).
[51]K. Nomura, H. Ohta, K. Ueda, T. Kamiya, M. Hirano, and H. Hosono, Science **300**, 1269 (2003).
[52]K. Nomura, T. Kamiya, H. Ohta, M. Hirano, and H. Hosono, Appl. Phys. Lett. **93**, 192107 (2008).
[53]K. Domen, T. Miyase, K. Abe, H. Hosono, and T. Kamiya, J. Disp. Technol. **10**, 975 (2015).
[54]S.-Y. Sung, J. H. Choi, U. B. Han, K. C. Lee, J.-H. Lee, J.-J. Kim, W. Lim, S. J. Pearton, D. P. Norton, and Y. W. Heo, Appl. Phys. Lett. **96**, 102107 (2010).
[55]W. Lim, E. A. Douglas, D. P. Norton, S. J. Pearton, F. Ren, Y. W. Heo, S. Y. Son, and J. H. Yuh, J. Vac. Sci. Technol. B **28**, 116 (2010).
[56]S. M. Kim, M.-J. Ahn, W.-J. Cho, and J. T. Park, Microelectron. Reliab. **64**, 575 (2016).
[57]J. H. Lee, S. K. Yu, J. W. Kim, M.-J. Ahn, and J. T. Park, Microelectron. Reliab. **64**, 580 (2016).
[58]W. Lim, J. H. Jang, S. H. Kim, D. P. Norton, V. Craciun, S. J. Pearton, F. Ren, and H. Shen, Appl. Phys. Lett. **93**, 082102 (2008).
[59]L. Qian and P. Lai, Microelectron. Reliab. **54**, 2396 (2014).
[60]J. K. Jeong, H. W. Yang, J. H. Jeong, Y. G. Mo, and H. D. Kim, Appl. Phys. Lett. **93**, 123508 (2008).
[61]Y. W. Heo, K. Cho, S. Sun, S. Kim, J. Lee, J. Kim, D. P. Norton, and S. J. Pearton, J. Vac. Sci. Technol. B **29**, 021203 (2011).
[62]J. G. Troughton, P. Downs, R. Price, and D. Atkinson, Appl. Phys. Lett. **110**, 011903 (2017).
[63]C.-Y. Chung, B. Zhu, R. G. Greene, M. O. Thompson, and D. G. Ast, Appl. Phys. Lett. **107**, 183503 (2015).
[64]K. Makise, K. Hidaka, S. Ezaki, T. Asano, B. Shinozaki, S. Tomai, K. Yano, and H. Nakamura, J. Appl. Phys. **116**, 153703 (2014).
[65]H.-C. Wu and C.-H. Chien, Appl. Phys. Lett. **102**, 062103 (2013).
[66]W.-H. Wang, S.-R. Lyu, E. Heredia, S.-H. Liu, P.-H. Jiang, P.-Y. Liao, T.-C. Chang, and H.-M. Chen, Appl. Phys. Lett. **110**, 022106 (2017).
[67]A. Kiazadeh, H. L. Gomes, P. Barquinha, J. Martins, A. Rovisco, J. V. Pinto, R. Martins, and E. Fortunato, Appl. Phys. Lett. **109**, 051606 (2016).
[68]P.-T. Liu, C.-H. Chang, and C.-J. Chang, Appl. Phys. Lett. **108**, 261603 (2016).
[69]S. Oh, J. H. Baeck, J. U. Bae, K.-S. Park, and I. B. Kang, Appl. Phys. Lett. **108**, 141604 (2016).
[70]K. Tsutsui, D. Matsubayashi, N. Ishihara, T. Takasu, S. Matsuda, and S. Yamazaki, Appl. Phys. Lett. **107**, 262104 (2015).
[71]K.-A. Kim, M.-J. Park, W.-H. Lee, and S.-M. Yoon, J. Appl. Phys. **118**, 234504 (2015).
[72]R. Kamal, P. Chandravanshi, D.-K. Choi, and S. M. Bobade, Curr. Appl. Phys. **15**, 648 (2015).
[73]K. A. Stewart, B.-S. Yeh, and J. F. Wager, J. Non-Cryst. Solids **455**, 102 (2017).
[74]L. Colalongo, Solid-State Electron. **124**, 1 (2016).
[75]K. Nomura, T. Kamiya, H. Ohta, T. Uruga, M. Hirano, and H. Hosono, Phys. Rev. B **75**, 35212 (2007).
[76]M. Orita, H. Tanji, M. Mizuno, H. Adachi, and I. Tanaka, Phys. Rev. B **61**, 1811 (2000).
[77]M. Orita, H. Ohta, M. Hirano, S. Narushima, and H. Hosono, Philos. Mag. B **81**, 501 (2001).
[78]A. Takagi, K. Nomura, H. Ohta, H. Yanagi, T. Kamiya, M. Hirano, and H. Hosono, Thin Solid Films **486**, 38 (2005).
[79]J. K. Jeong, J. H. Jeong, J. H. Choi, J. S. Im, S. H. Kim, H. W. Yang, K. N. Kang, K. S. Kim, T. K. Ahn, H.-J. Chung, M. Kim, B. S. Gu, J.-S. Park, Y.-G. Mo, H. D. Kim, and H. K. Chung, Tech. Dig. - SID Int. Symp. **39**, 1 (2008).
[80]H. Hosono, J. Non-Cryst. Solids **352**, 851 (2006).
[81]H. Hosono, N. Kikuchi, N. Ueda, and H. Kawazoe, J. Non-Cryst. Solids **198**, 165 (1996).
[82]H. Hosono, M. Yasukawa, and H. Kawazoe, J. Non-Cryst. Solids **203**, 334 (1996).
[83]M. J. Powell, B. C. Easton, and D. H. Nicholls, J. Appl. Phys. **53**, 5068 (1982).
[84]T. C. Fung, C. S. Chuang, K. Nomura, H. P. D. Shieh, H. Hosono, and J. Kanicki, J. Inf. Disp. **9**, 21 (2008).
[85]W. Lim, S. H. Kim, Y. L. Wang, J. W. Lee, D. P. Norton, S. J. Pearton, F. Ren, and I. Kravchenko, J. Electrochem. Soc. **155**, H383 (2008).
[86]B. D. Ahn, H.-S. Kim, D.-J. Yun, J.-S. Park, and H. J. Kim, ECS J. Solid State Sci. Technol. **3**, Q95 (2014).
[87]K. Domen, T. Miyase, K. Abe, H. Hosono, and T. Kamiya, IEEE Electron Devices Lett. **35**, 832 (2013).
[88]T. Miyase, K. Watanabe, I. Sakaguchi, N. Ohashi, K. Domen, K. Nomura, H. Hiramatsu, H. Kumomi, H. Hosono, and T. Kamiya, ECS J. Solid State Sci. Technol. **3**, Q3085 (2014).

[89]Y. Hanyu, K. Domen, K. Nomura, H. Hiramatsu, H. Kumomi, H. Hosono, and T. Kamiya, Appl. Phys. Lett. **103**, 202114 (2013).
[90]S. Kwon, J. H. Noh, J. Noh, and P. D. Rack, J. Electrochem. Soc. **158**, H289 (2011).
[91]M. N. Fujii, Y. Ishikawa, M. Horita, and Y. Uraoka, ECS J. Solid State Sci. Technol. **3**, Q3050 (2014).
[92]Y.-H. Joo, J.-C. Woo, and C.-I. Kim, J. Electrochem. Soc. **159**, D190 (2012).
[93]Y. W. Lee, S.-J. Kim, S.-Y. Lee, W.-G. Lee, K.-S. Yoon, J.-W. Park, and M.-K. Han, Electrochem. Solid-State Lett. **15**, H84 (2012).
[94]J. Robertson and C. W. Chen, Appl. Phys. Lett. **74**, 1168 (1999).
[95]J. Robertson, J. Vac. Sci. Technol. B **18**, 1785 (2000).
[96]J. Robertson, MRS Bull. **27**, 217 (2002).
[97]Z. W. Zheng, C. H. Cheng, and Y. C. Chen, ECS J. Solid State Sci. Technol. **2**, N179 (2013).
[98]K. Kurishima, T. Nabatame, M. Shimizu, S. Aikawa, K. Tsukagoshi, A. Ohi, T. Chikyo, and A. Ogura, ECS Trans. **61**, 345 (2014).
[99]H. Lim, H. Yin, J.-S. Park, I. Song, C. Kim, J. Park, S. Kim, S.-W. Kim, C. B. Lee, Y. C. Kim, Y. S. Park, and D. Kang, Appl. Phys. Lett. **93**, 063505 (2008).
[100]W. Lim, Y. L. Wang, J. Lee, D. P. Norton, F. Ren, and S. J. Pearton, ECS Trans. **16**, 303 (2008).
[101]Y.-J. Chen and Y.-H. Tai, ECS Solid State Lett. **4**, Q10 (2015).
[102]M. P. Hung, D. Wang, and M. Furuta, ECS Solid State Lett. **4**, Q66 (2015).
[103]M. Nag, A. Bhoolokam, S. Steudel, J. Genoe, G. Groeseneken, and P. Heremans, ECS J. Solid State Sci. Technol. **4**, N99 (2015).
[104]T. M. Pan, C. H. Chen, J. H. Liu, F. H. Chen, J. L. Her, and K. Koyama, IEEE Trans. Electron Devices **61**, 87 (2014).
[105]J. S. Lee, S. Chang, S. M. Koo, and S. Y. Lee, IEEE Electron Device Lett. **31**, 225 (2010).
[106]C. J. Chiu, S. P. Chang, and S. J. Chang, IEEE Electron Device Lett. **31**, 1245 (2010).
[107]H. Q. Chiang, B. R. McFarlane, D. Hong, R. E. Presley, and J. F. Wager, J. Non-Cryst. Solids **354**, 2826 (2008).
[108]Y. J. Cho, J. H. Shin, S. M. Bobade, Y. B. Kim, and D. K. Choi, Thin Solid Films **517**, 4115 (2009).
[109]H. Kumomi, K. Nomura, T. Kamiya, and H. Hosono, Thin Solid Films **51**, 1516 (2008).
[110]X. Ding, H. Zhang, J. Zhang, J. Li, W. Shi, X. Jiang, and Z. Zhang, Mater. Sci. Semicond. Process. **29**, 69 (2015).
[111]H. H. Hsu, C. Y. Chang, C. H. Cheng, S. H. Yu, C. Y. Su, and C. Y. Su, Solid-State Electron. **89**, 194 (2013).
[112]C. J. Chiu, S. P. Chang, C. Y. Lu, P. Y. Su, and S. J. Chang, AIP Conf. Proc. **1399**, 929 (2011).
[113]J. C. Park, K.-W. Kim, J. W. Lee, B. P. Gila, D. P. Norton, F. Ren, S. J. Pearton, O. G. Jeong, T. G. Kim, J. K. Kim, and H. Cho, J. Ceram. Proc. Res. **15**, 545 (2014).
[114]D. C. Hays, B. P. Gila, S. J. Pearton, B.-J. Kim, F. Ren, and T. S. Jang, J. Vac. Sci. Technol. B **33**, 051218 (2015).
[115]J. C. Park, K. Kim, B. P. Gila, E. S. Lambers, D. P. Norton, S. J. Pearton, F. Ren, J. K. Kim, and H. Cho, J. Nanosci. Nanotechnol. **14**, 8445 (2014).
[116]D. C. Hays, B. P. Gila, S. J. Pearton, B.-J. Kim, and F. Ren, Vacuum **125**, 113 (2016).
[117]D. C. Hays, B. P. Gila, S. J. Pearton, and F. Ren, ECS J. Solid State Sci. Technol. **5**, P680 (2016).
[118]G. He, X. F. Chen, J. G. Lv, Z. B. Fang, Y. M. Liu, K. R. Zhu, Z. Q. Sun, and M. Liu, J. Alloys Compd. **642**, 172 (2015).
[119]S. Heo, J. Chung, J. C. Lee, T. Song, S. H. Kim, D.-J. Yun, H. I. Lee, K. Kim, G. S. Park, J. S. Oh, D. W. Kwak, D. Lee, H. Y. Cho, D. Tahi, H. J. Kang, and B.-D. C. Heo, Surf. Interface Anal. **48**, 1062 (2016).
[120]X. F. Chen, G. He, J. G. Lv, M. Liu, P. H. Wang, X. S. Chen, and Z. Q. Sun, J. Alloys Compd. **647**, 1035 (2015).
[121]K. Lee, K. Nomura, H. Yanagi, T. Kamiya, E. Ikenaga, T. Sugiyama, K. Kobayashi, and H. Hosono, J. Appl. Phys. **112**, 033713 (2016).
[122]Z.-Y. Xie, H.-L. Lu, S.-S. Xu, Y. Geng, Q.-Q. Sun, S.-J. Ding, and D. W. Zhang, Appl. Phys. Lett. **101**, 252111 (2012).
[123]E. A. Kraut, R. W. Grant, J. R. Waldrop, and S. P. Kowalczyk, Phys. Rev. Lett. **44**, 1620 (1980).
[124]D. A. Shirley, Phys. Rev. B **5**, 4709 (1972).
[125]R. S. List and W. E. Spicer, J. Vacuum Sci. Technol. B **6**, 1228 (2016).
[126]S. Tougaard, Surf. Sci. **216**, 343 (1989).
[127]S. Tougaard and C. Jansson, Surf. Interface Anal. **20**, 1013 (1993).
[128]P. Poveda and A. Glachant, J. Non-Cryst. Solids **216**, 83 (1997).
[129]S. Tougaard, J. Vac. Sci. Technol. A **8**, 2197 (1990).
[130]S. Tougaard, J. Vac. Sci. Technol. A **5**, 1230 (1987).
[131]J. B. Clemens, S. R. Bishop, J. S. Lee, A. C. Kummel, and R. Droopad, J. Chem. Phys. **132**, 244701 (2010).
[132]D. Briggs, *Surface Analysis of Polymers by XPS and Static SIMS* (Cambridge University Press, Cambridge, U.K., 1998), p. 198.
[133]W. S. M. Werner, Surf. Interface Anal. **31**, 141 (2001).
[134]M. T. Nichols, W. Li, D. Pei, G. A. Antonelli, Q. Lin, S. Banna, Y. Nishi, and J. L. Shohetless, J. Appl. Phys. **115**, 094105 (2014).
[135]D. Penn, Phys. Rev. Lett. **38**, 1429 (1977).
[136]S. Hügner, *Photoelectron Spectroscopy: Principles and Applications* (Springer, 2003).
[137]H. Jin, H. Shinotsuka, H. Yoshikawa, H. Iwai, S. Tanuma, and S. Tougaard, J. Appl. Phys. **107**, 083709 (2010).
[138]P. Risterucci, O. Renault, E. Martinez, B. Detlefs, V. Delaye, J. Zegenhagen, C. Gaumer, G. Grenet, and S. Tougaard, Appl. Phys. Lett. **104**, 051608 (2014).
[139]E. Bersch, M. Di, S. Consiglio, R. D. Clark, G. J. Leusink, and A. C. Diebold, J. Appl. Phys. **107**, 043702 (2010).
[140]G. D. Wilk and D. A. Muller, Appl. Phys. Lett. **83**, 3984 (2003).
[141]E. Bersch, S. Rangan, R. A. Bartynski, E. Garfunkel, and E. Vescovo, Phys. Rev. B **78**, 085114 (2008).
[142]C. C. Fulton, G. Lucovsky, and R. J. Nemanich, Appl. Phys. Lett. **84**, 580 (2004).
[143]Z. L. Wang and J. M. Cowley, Surf. Sci. **193**, 501 (1988).
[144]Z. L. Wang and J. Bentley, Microsc. Res. Tech. **20**, 390 (1992).
[145]Z. L. Wang, J. Electron Microsc. Tech. **14**, 13 (1990).
[146]R. F. Egerton, *Electron Energy Loss Spectroscopy in the Electron Microscope* (Plenum Press, New York, 1996).
[147]J. C. H. Spence, Rep. Prog. Phys. **69**, 725 (2006).
[148]S. Ren and M. Caricato, J. Chem. Phys. **144**, 184102 (2016).
[149]J. R. Waldrop, S. P. Kowalczyk, R. W. Grant, E. A. Kraut, and D. L. Miller, J. Vac. Sci. Technol. **19**, 573 (1981).
[150]R. Puthenkovilakam, E. A. Carter, and J. P. Chang, Phys. Rev. B **69**, 155329 (2004).
[151]V. K. Adamchuk and V. V. Afanas'ev, Prog. Surf. Sci. **41**, 111 (1992).
[152]V. V. Afanas'ev, M. Bassler, G. Pensl, M. J. Schulz, and E. Stein von Kamienski, J. Appl. Phys. **79**, 3108 (1996).
[153]E. A. Kraut, R. W. Grant, J. R. Waldrop, and S. P. Kowalczyk, Phys. Rev. B **28**, 1965 (1983).
[154]J. Strait and J. Tauc, Appl. Phys. Lett. **47**, 589 (1985).
[155]J. Tauc, Phys. Today **29**(15), 23 (1976).
[156]Y. Feng, S. Lin, S. Huang, S. Shrestha, and G. Conibeer, J. Appl. Phys. **117**, 125701 (2015).
[157]H. Oheda, J. Appl. Phys. **92**, 195 (2002).
[158]Z. Vardeny, J. Strait, and J. Tauc, Appl. Phys. Lett. **42**, 580 (1983).
[159]T. E. Cook, C. C. Fulton, W. J. Mecouch, K. M. Tracy, R. F. Davis, E. H. Hurt, G. Lucovsky, and R. J. Nemanich, J. Appl. Phys. **93**, 3995 (2003).
[160]L. J. Brillson, Surf. Sci. **299**, 909 (1994).
[161]K. L. Chopra, *Thin Film Phenomena* (R. E. Krieger Pub. Co., Huntington, NY, 1979).
[162]J. L. Vossen and W. Kern, *Thin Film Processes II* (Academic Press, Boston, 1991).
[163]J. S. Chapin, "Sputtering process and apparatus," Res. Dev. Mag. **25**, 37 (1974).
[164]A. Rockett, *The Materials Science of Semiconductors* (Springer, NY, 2008), p. 505.
[165]B. S. Probyn, Vacuum **18**, 253 (1968).
[166]J. S. Logan, N. M. Mazza, and P. D. Davidse, J. Vac. Sci. Technol. **6**, 120 (1969).
[167]G. N. Jackson, Thin Solid Films **5**, 209 (1970).
[168]D. L. Smith, *Thin-Film Deposition: Principles and Practice* (McGraw-Hill, New York, 1995).
[169]R. L. Puurunen, J. Appl. Phys. **97**, 121301 (2005).
[170]S. Langereis, S. Heil, H. Knoops, W. Keuning, M. van de Sanden, and W. Kessels, J. Phys. D: Appl. Phys. **42**, 073001 (2009).
[171]J. Zaera, J. Phys. Chem. Lett. **3**, 1301 (2012).
[172]M. Miikkulainen, M. Leskelä, M. Ritala, and R. Puurunen, J. Appl. Phys. **113**, 021301 (2013).
[173]G. Moore, Electronics **38**, 144 (1965).
[174]G. E. Moore, Tech. Dig. - IEEE Int. Solid-State Circuits Conf. **1**, 20 (2003).
[175]M. Depas, B. Vermeire, P. W. Mertens, R. L. van Meihaeghe, and M. M. Heyns, Solid-State Electron. **38**, 1465 (1995).

[176]A. I. Kingon and S. K. Streiffer, Nature **406**, 1032 (2000).
[177]G. D. Wilk, R. M. Wallace, and J. M. Anthony, J. Appl. Phys. **89**, 5243 (2001).
[178]A. Franciosi and C. van de Walle, Surf. Sci. Rep. **25**, 1 (1996).
[179]M. Peressi, N. Binggeli, and A. Baldereschi, J. Phys. D: Appl. Phys. **31**, 1273 (1998).
[180]E. A. Douglas, A. Scheurmann, R. P. Davies, B. P. Gila, H. Cho, V. Craciun, E. S. Lambers, S. J. Pearton, and F. Ren, Appl. Phys. Lett. **98**, 242110 (2011).
[181]D. Tahir, S. D. A. Ilyas, and H. J. Kang, Makara J. Sci. **15**, 193 (2011).
[182]H. Cho, E. A. Douglas, A. Scheurmann, B. P. Gila, V. Craciun, E. S. Lambers, S. J. Pearton, and F. Ren, Electrochem. Solid-State Lett. **14**, H431 (2011).
[183]J. Yao, S. Zhang, and L. Gong, Appl. Phys. Lett. **101**, 093508 (2012).
[184]J. K. Kim, K.-W. Kim, E. A. Douglas, B. P. Gila, V. Craciun, E. S. Lambers, D. P. Norton, F. Ren, S. J. Pearton, and H. Cho, J. Nanosci. Nanotechnol. **14**, 3925 (2014).
[185]H. C. Shin, D. Tahir, S. Seo, Y. R. Denny, S. K. Oh, H. J. Kang, S. Heo, J. G. Chung, J. C. Lee, and S. Tougaard, Surf. Interface Anal. **44**, 623 (2012).
[186]S. J. Pearton, D. P. Norton, K. Ip, Y. W. Heo, and T. Steiner, Prog. Mater. Sci. **50**, 293 (2005).
[187]H. Y. Huang, Y. C. Huang, J. Y. Su, N. C. Su, C. K. Chiang, C. H. Wu, and S. J. Wang, in *68th Device Research Conference* (2010), p. 235.
[188]D. C. Hays, B. P. Gila, S. J. Pearton, and F. Ren, Vacuum **116**, 60 (2015).
[189]Y. Chung, H. Park, S. B. Cho, Y. S. Yoon, and D. J. Kim, J. Ceram. Process. Res. **15**, 331 (2014).
[190]E. A. Paisley, M. Brumbach, A. A. Allerman, S. Atcitty, A. G. Baca, A. M. Armstrong, R. J. Kaplar, and J. F. Ihlefeld, Appl. Phys Lett. **107**, 102101 (2015).
[191]H. S. Craft, R. Collazo, M. D. Losego, S. Mita, Z. Sitar, and J. P. Maria, J. Appl. Phys. **102**, 074104 (2007).
[192]J. J. Chen, B. P. Gila, M. Hlad, A. Gerger, F. Ren, C. R. Abernathy, and S. J. Pearton, Appl. Phys. Lett. **88**, 042113 (2006).
[193]P. Barquinha, L. Pereira, G. Gonçalves, R. Martins, and E. Fortunato, J. Electrochem. Soc. **156**, H161 (2009).
[194]D. Kang, I. Song, C. Kim, Y. Park, T. D. Kang, H. S. Lee, J.-W. Park, S. H. Baek, S.-H. Choi, and H. Lee, Appl. Phys. Lett. **91**, 091910 (2007).
[195]A. Kaiser, M. Lobert, and R. Telle, J. Eur. Ceram. Soc. **28**, 2199 (2008).
[196]P. W. Peacock and J. Robertson, J. Appl. Phys. **92**, 4712 (2002).
[197]J. Robertson, Rep. Prog. Phys. **69**, 327 (2005).
[198]S. Sayan, N. V. Nguyen, J. Ehrstein, T. Emge, E. Garfunkel, M. Croft, X. Zhao, D. Vanderbilt, I. Levin, E. P. Gusev, H. Kim, and P. J. McIntyre, Appl. Phys. Lett. **86**, 152902 (2005).
[199]L. X. Qian, X. Z. Liu, C. Y. Han, and P. T. Lai, IEEE Trans. Device Mater. Reliab. **14**, 1056 (2014).
[200]D. C. Hays, B. P. Gila, S. J. Pearton, and F. Ren, Vacuum **122**, 195 (2015).
[201]H. Cho, E. A. Douglas, B. P. Gila, V. Craciun, E. S. Lambers, F. Ren, and S. J. Pearton, Appl. Phys. Lett. **100**, 012105 (2012).
[202]C. Besleaga, G. E. Stan, I. Pintilie, P. Barquinha, E. Fortunato, and R. Martins, Appl. Surf. Sci. **379**, 270 (2016).
[203]A. M. Herrero, B. P. Gila, A. Gerger, A. Scheuermann, R. Davies, C. R. Abernathy, S. J. Pearton, and F. Ren, J. Appl. Phys. **106**, 074105 (2009).
[204]B. P. Gila, M. Hlad, A. H. Onstine, R. Frazier, G. T. Thaler, A. Herrero, E. Lambers, C. R. Abernathy, S. J. Pearton, T. Anderson, S. Jang, F. Ren, N. Moser, R. C. Fitch, and M. Freund, Appl. Phys. Lett. **87**, 163503 (2005).
[205]A. M. Herrero, B. P. Gila, C. R. Abernathy, S. J. Pearton, V. Craciun, K. Siebein, and F. Ren, Appl. Phys. Lett. **89**, 092117 (2006).
[206]D. C. Hays, B. P. Gila, S. J. Pearton, A. Trucco, R. Thorpe, and F. Ren, J. Vac. Sci. Technol. B **35**, 011206 (2017).
[207]F. L. Martınez, M. Toledano-Luque, J. J. Gandia, J. Carabe, W. Bohne, J. Rohrich, E. Strub, and I. Martil, J. Phys. D: Appl. Phys. **40**, 5256 (2007).
[208]T. Tan, Z. Liu, H. Lu, W. Liu, F. Yan, and W. Zhang, Appl. Phys. A **97**, 475 (2009).
[209]D. Hays, B. P. Gila, F. Ren, and S. J. Pearton, J. Vac. Sci. Technol. B **33**, 061209 (2015).
[210]C. Y. Zheng, G. He, X. F. Chen, M. Liu, J. G. Lv, J. Gao, J. W. Zhang, D. Q. Xiao, P. Jin, S. S. Jiang, W. D. Li, and Z. Q. Sun, J. Alloys Compd. **679**, 115 (2016).
[211]A. Munoz, R. Perez, J. C. Duran, and F. Flores, Surf. Sci. **211/212**, 503 (1989).
[212]A. Klein, J. Phys. C: Solid State Phys. **27**, 134201 (2015).
[213]J. Robertson and S. J. Clark, Phys. Rev. B **83**, 075205 (2011).
[214]F. Chen, R. Schafranek, S. Li, W. Wu, and A. J. Klein, J. Phys. D: Appl. Phys. **43**, 295301 (2010).
[215]S. Li, F. Chen, R. Schafranek, T. J. M. Bayer, K. Rachut, A. Fuchs, S. Siol, M. Weidner, M. Hohmann, V. Pfeifer, J. Morasch, C. Ghinea, E. Arveux, R. Gunzler, J. Gassmann, C. Korber, Y. Gassenbauer, F. Sauberlich, G. V. Rao, S. Payan, M. Maglione, C. Chirila, L. Pintilie, L. Jia, K. Ellmer, M. Naderer, K. Reichmann, U. Bottger, S. Schmelzer, R. C. Frunza, H. Ursic, B. Malic, W.-B. Wu, P. Erhart, and A. Klein, Phys Status Solidi RRL **8**, 571 (2014).
[216]A. Klein, Thin Solid Films **520**, 3721 (2012).
[217]C. G. Van de Walle and L. H. Yang, J. Vac. Sci. Technol. B **13**, 1635 (1995).
[218]R. Southwick and W. Knowlton, IEEE Trans. Device Mater. Reliab. **6**, 136 (2006).
[219]R. G. Southwick, A. Sup, A. Jain, and W. B. Knowlton, IEEE Trans. Device Mater. Reliab. **11**, 236 (2011).
[220]M. J. Mutch, T. Pomorski, B. C. Bittel, C. J. Cochrane, P. M. Lenahan, X. Liu, R. J. Nemanich, J. Brockman, M. French, M. Kuhn, B. French, and S. W. King, Microelectron. Reliab. **63**, 201 (2016).
[221]L. Kim, J. Kim, U. V. Waghmare, D. Jung, and J. Lee, Phys. Rev. B **72**, 214121 (2005).
[222]W. D. Kingery, H. K. Bowen, and D. R. Uhlmann, *Introduction to Ceramics* (John Wiley & Sons, New York), p. 913.
[223]C. M. Brooks, L. F. Kourkoutis, T. Heeg, J. Schubert, D. A. Muller, and D. G. Schlom, Appl. Phys. Lett. **94**, 162905 (2009).
[224]S. Balaz, Z. Zeng, and L. J. Brillson, J. Appl. Phys. **114**, 183701 (2013).
[225]J. Morais, E. B. O. da Rosa, L. Miotti, R. P. Pezzi, I. J. R. Baumvol, A. L. P. Rotondaro, M. J. Bevan, and L. Colombo, Appl. Phys. Lett. **78**, 2446 (2001).
[226]See http://xpssimplified.com/periodictable.php for "Thermo Scientific X-Ray Photoelectron Spectroscopy XPS" (last accessed January 14, 2017).
[227]X. Guo, H. Zheng, S. W. King, V. V. Afanas'ev, M. R. Baklanov, J.-F. D. Marneffe, Y. Nishi, and J. L. Shohet, Appl. Phys. Lett. **107**, 139903 (2015).
[228]A. Zur and T. C. McGill, J. Vac. Sci. Technol. B **2**, 440 (1984).
[229]H.-K. Dong and L.-B. Shi, Chin. Phys. Lett. **33**, 016101 (2016).
[230]J. Xu, Y. Teng, and F. Teng, Sci. Rep. **6**, 32457 (2016).
[231]M. Yang, R. Q. Wu, Q. Chen, W. S. Deng, Y. P. Feng, J. W. Chai, J. S. Pan, and S. J. Wang, Appl. Phys. Lett. **94**, 142903 (2009).
[232]S. Rahimnejad, J. H. He, W. Chen, K. Wu, and G. Q. Xu, RSC Adv. **4**, 62423 (2014).
[233]W R. Runyan, *Semiconductor Measurements and Instrumentation* (McGraw-Hill, Tokyo, 1975), p. 48.
[234]A. K. Rumaiz, B. Ali, A. Ceylan, M. Boggs, T. Beebe, and S. I. Shah, Solid State Commun. **144**, 334 (2007).
[235]S. Heo, E. Cho, H.-I. Lee, G. S. Park, H. J. Kang, T. Nagatomi, P. Choi, and B.-D. Choi, AIP Adv. **5**, 077167 (2015).
[236]S. King, B. French, and E. Mays, J. Appl. Phys. **113**, 044109 (2013).
[237]B. French and S. W. King, J. Mater. Res. **28**, 2771 (2013).
[238]C. Priester, G. Allan, and M. Lannoo, J. Vac. Sci. Technol. B **6**, 1290 (1988).
[239]W. Yang, M. Fronk, Y. Geng, L. Chen, Q.-Q. Sun, O. D. Gordan, P. Zhou, D. R. Zahn, and D. W. Zhang, Nanoscale Res. Lett. **10**, 1 (2015).
[240]H. Jin, S. K. Oh, H. J. Kang, and M.-H. Cho, Appl. Phys. Lett. **89**, 122901 (2006).
[241]H. Kato, T. Nango, T. Miyagawa, T. Katagiri, K. S. Seol, and Y. Ohki, J. Appl. Phys. **92**, 1106 (2002).
[242]J. S. Lee, J. D. Lim, Z. G. Khim, Y. D. Park, S. J. Pearton, and S. N. G. Chu, J. Appl. Phys. **93**, 4512 (2003).
[243]J. Robertson, J. Vac. Sci. Technol. **31**, 050821 (2013).
[244]J. Robertson, Rep. Prog. Phys. **69**, 327 (2006).
[245]X. Wang, O. Saadat, B. Xi, X. Lou, R. Molnar, T. Palacios, and R. Gordon, Appl. Phys. Lett. **101**, 232109 (2012).
[246]W. Qi, R. Nieh, E. Dharmarajan, B. Lee, Y. Jeon, L. Kang, K. Onishi, and J. Lee, Appl. Phys. Lett. **77**, 1704 (2000).
[247]J. Zhang, Y. Li, B. Zhang, H. Wang, Q. Xin, and A. Song, Nat. Commun. **6**, 7561 (2015).
[248]S. Rha, J. Jung, Y. Jung, Y. Chung, U. Kim, E. Hwang, B. Park, T. Park, J. Choi, and C. Hwang, IEEE Trans. Electron Devices **59**, 3357 (2012).
[249]J. Wager, B. Yeh, R. Hoffman, and D. Keszler, Curr. Opin. Solid State Mater. Sci. **18**, 53 (2014).